AIR FORCE REPORT NO.
SAMSO-TR-71-166

AEROSPACE REPORT NO.
TR-0059(6784)-1

Configuration Studies for Autonomous Satellite Navigation

Prepared by I. A. GURA, A. S. ABBOTT, and H. T. HENDRICKSON
Electronics Division

71 MAY 28

Engineering Science Operations
THE AEROSPACE CORPORATION

Prepared for SPACE AND MISSILE SYSTEMS ORGANIZATION
AIR FORCE SYSTEMS COMMAND
LOS ANGELES AIR FORCE STATION
Los Angeles, California

UNCLASSIFIED
Security Classification

DOCUMENT CONTROL DATA - R & D
(Security classification of title, body of abstract and indexing annotation must be entered when the overall report is classified)

1. ORIGINATING ACTIVITY (Corporate author) The Aerospace Corporation El Segundo, California 90245	2a. REPORT SECURITY CLASSIFICATION UNCLASSIFIED 2b. GROUP

3. REPORT TITLE

CONFIGURATION STUDIES FOR AUTONOMOUS SATELLITE NAVIGATION

4. DESCRIPTIVE NOTES (Type of report and inclusive dates)

5. AUTHOR(S) (First name, middle initial, last name)

Ira A. Gura
Anthony S. Abbott
Howard T. Hendrickson

6. REPORT DATE	7a. TOTAL NO. OF PAGES	7b. NO. OF REFS
71 MAY 28	111	52

8a. CONTRACT OR GRANT NO.	9a. ORIGINATOR'S REPORT NUMBER(S)
F04701-70-C-0059	TR-0059(6784)-1
b. PROJECT NO.	
c.	9b. OTHER REPORT NO(S) (Any other numbers that may be assigned this report)
d.	SAMSO-TR-71-166

10. DISTRIBUTION STATEMENT

Approved for public release; distribution unlimited.

11. SUPPLEMENTARY NOTES	12. SPONSORING MILITARY ACTIVITY
	Space and Missile Systems Organization Air Force Systems Command Los Angeles, California 90045

13. ABSTRACT

Several autonomous satellite navigation configurations were studied on a common low-altitude basis with the emphasis on accuracy and convergence. Analysis was performed by simulations using recursive filtering techniques. Configurations investigated included horizon sensors, unknown landmark tracking, known landmark tracking, and one-way doppler systems. Relevant sensor combinations were analyzed to determine possible performance augmentation.

DD FORM (FACSIMILE) 1473

UNCLASSIFIED
Security Classification

14 KEY WORDS

Navigation
Filtering
Sensor
Satellite
Orbit Determination
Simulation
Autonomous Navigation
Onboard Computing
Kalman Filtering
Unknown Landmark Tracking
Known Landmark Tracking
Horizon Sensors
One-way Doppler systems

Distribution Statement (Continued)

Abstract (Continued)

Air Force Report No.
SAMSO-TR-71-166

Aerospace Report No.
TR-0059(6784)-1

CONFIGURATION STUDIES FOR AUTONOMOUS SATELLITE NAVIGATION

Prepared by

I. A. Gura, A. S. Abbott, and H. T. Hendrickson
Electronics Division

71 MAY 28

Engineering Science Operations
THE AEROSPACE CORPORATION

Prepared for

SPACE AND MISSILE SYSTEMS ORGANIZATION
AIR FORCE SYSTEMS COMMAND
LOS ANGELES AIR FORCE STATION
Los Angeles, California

FOREWORD

This report is published by The Aerospace Corporation, El Segundo, California, under Air Force Contract No. F04701-70-C-0059. This report was authored by Ira A. Gura and Howard T. Hendrickson of the Satellite Navigation Department, Guidance and Navigation Subdivision, and by Anthony S. Abbott of the Control Systems Department, Control and Sensor Systems Subdivision, Electronics Division, Engineering Science Operations.

This report, which documents research carried out from January 1971 through May 1971, was submitted for review and approval on 28 June 1971 to SAMSO (SYGS).

This report contains no classified information extracted from classified documents.

Approved by

J. E. Farr, Director
Program 681D
Control and Sensor Systems
Subdivision
Electronics Division

A. J. Schiewe, Director
Control and Sensor Systems
Subdivision
Electronics Division

M. T. Weiss, General Manager
Electronics Division
Engineering Science Operations

Publication of this report does not constitute Air Force approval of the report's findings or conclusions. It is published only for the exchange and stimulation of ideas.

Herbert A Briesacher
Major, USAF
681D Program Manager

ABSTRACT

Several autonomous satellite navigation configurations were studied on a common low-altitude basis with the emphasis on accuracy and convergence. Analysis was performed by simulations using recursive filtering techniques. Configurations investigated included horizon sensors, unknown landmark tracking, known landmark tracking, and one-way doppler systems. Relevant sensor combinations were analyzed to determine possible performance augmentation.

CONTENTS

CONTENTS (Continued)

FIGURES

TABLES

TABLES (Continued)

1. INTRODUCTION

This report documents a four-month study on autonomous satellite navigation in which various sensors were compared on a uniform basis. Special attention was given to possible hybrid configurations for optimizing autonomy, accuracy, simplicity, and time of convergence. A special computer program called SNAP (Space Navigation Analysis Program) was developed for analysis of the various systems. Comparisons were made on the basis of simulation results for a low altitude satellite orbit. Among the sensor types considered were unknown landmark tracking, known landmark tracking, horizon sensors and one-way doppler systems. The work of previous investigators in these areas (Refs. 1, 5, 6, 7, 20, 21, 22, 23, 24, 27, 33, 35, and 41) was used in developing appropriate system models and in choosing the parameters for the cases considered.

The conclusions obtained in this study are, of course, influenced by the specific configurations analyzed and the low altitude orbit used. Hence, care should be exercised in extrapolating the results reported herein to other situations.

2. SIMULATION SOFTWARE

The various sensor configurations considered in this study were evaluated by means of processing simulated sensor data via a suitable estimation algorithm. The Aerospace Corporation has extensive software capabilities for performing such analyses. Among the available programs are TRACE (Refs. 9 and 42), MVS (Ref. 39), ONUMS (Ref. 1) and ONAP (Refs. 25, 26, and 36). The latest program, SNAP, was specifically designed for this study to facilitate simulation of hybrid sensor systems. The basic simulation logic used is shown schematically in Fig. 2-1. Some of the principle features of this program are highlighted below.

2.1 By means of a simple input flag, the user can choose between Standard Kalman, Stabilized Kalman or Andrews square-root filtering algorithms (Ref. 2 and 18). The Andrews filter is a generalization of an approach originally suggested by Potter (Ref. 3). Dynamic "forcing noise" can be accommodated with square-root filtering by use of either a Cholesky or a Householder decomposition.

2.2 In order to simplify programming, all partial derivatives are computed numerically. While analytic partials are generally more desirable in a specific application, the numerical technique was used to provide flexibility as simulation demands changed. In a limited number of test cases, the results obtained using this approach compared quite well with the results of other software which was based on the analytic approach to partial derivative computations.

2.3 The dynamic models to be used for any run can be chosen from any of the following "real world" or "filter world" options:

Real World Models (See Appendix A)

Keplerian, no atmosphere
Keplerian, U.S. Standard Atmosphere, 1962
APL "8-8" geopotential, no atmosphere
APL "8-8" geopotential, U.S. Standard Atmosphere, 1962

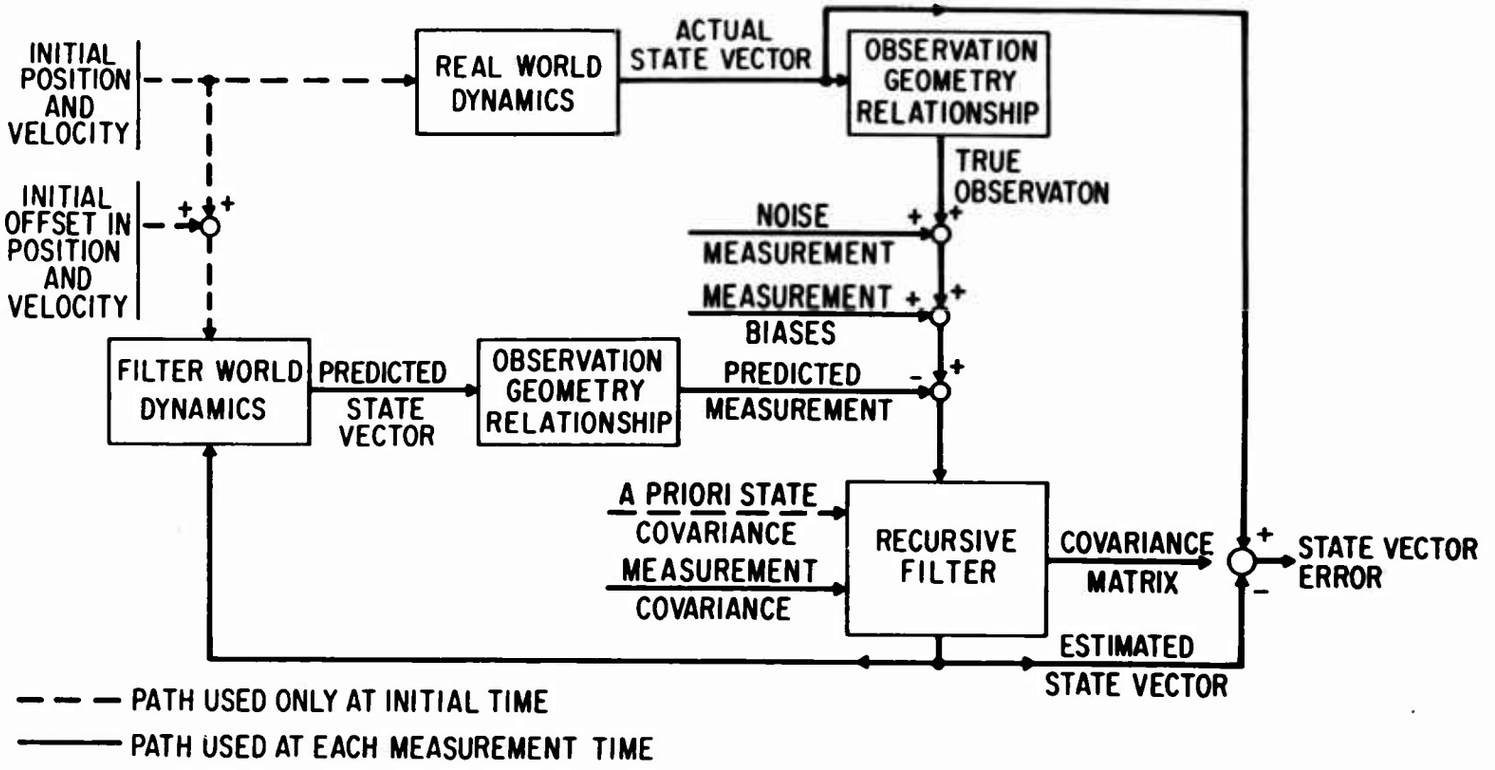

Figure 2-1. Simulation Procedures

Filter World Models (See Appendix B)

Keplerian, no atmosphere
Keplerian, exponential atmosphere
μ and J_2 geopotential, no atmosphere
μ and J_2 geopotential, exponential atmosphere

These models were chosen primarily to provide a reasonable mismatch between the real world and filter world emphemeris (Refs. 5, 6, 21, 22, 23, 24). Extensive investigation would clearly be required to determine optimum filter world models for an operational system.

2.4 A simple array of integers specified at execution time is used to establish the elements of the state vector to be estimated for a particular case.

2.5 Configurations for autonomous navigation can be chosen from among the sensor options listed below by an appropriate array of integers. Up to three independent sensors of any specific type can be used simultaneously, with the number of different types chosen for any configuration limited only by the rationality of the final system. Furthermore, an independent measurement schedule can be provided for each sensor chosen. As required, any sensor observation can be biased with or without that quantity appearing in the state vector.

Sensor Options in SNAP

1. Azimuth and elevation to unknown landmark
2. Horizon sensor (direction to center of earth, angle subtended by disk of earth)
3. Azimuth and elevation to known landmark
4. Range, azimuth, and elevation to known landmark
5. Range to known landmark
6. Range rate to known landmark
7. One-way doppler to known landmark
8. Star elevation above earth horizon

9. Range to satellite
10. Azimuth and elevation to satellite
11. Range, azimuth, and elevation to satellite
12. Range rate to satellite
13. Range difference between two satellites
14. Range rate difference between two satellites
15. Range difference between two known landmarks
16. Range rate difference between two known landmarks
17. Radar altimeter

Since the total time available for this study was quite limited, no attempt was made to evaluate all of the above sensor systems. Specifically, only options 1 through 7 were examined in this study.

3. BASIC ASSUMPTIONS AND PROCEDURES

In order to provide a uniform basis of comparison for the systems considered, the following basic assumptions and procedures were used in all the simulation studies:

3.1 The basic simulation procedure used for all studies is shown schematically in Fig. 2-1.

3.2 A reference orbit having a nominal 80 n mi perigee and a 200 n mi apogee was used. This orbit was arbitrarily chosen as typical of low-altitude orbits. Detailed orbital conditions are given in Appendix C.

3.3 Unless otherwise specified, real world data were generated using the APL "8-8" geopotential and the 1962 U.S. Standard Atmosphere models described in Appendix A. All filter calculations were based on the $\mu - J_2$ geopotential and the exponential atmosphere models described in Appendix B.

3.4 Since the total time available for the study was quite limited, no attempt was made to compensate for dynamic model errors. Where possible, however, an approximate point of divergence was identified. Note that the basic problem of compensating for model mismatches has been shown to be solvable empirically (Refs. 6, 22), generally requiring extensive analysis and simulation for a specific configuration.

3.5 Because of recent advances in attitude reference systems (Refs. 10 and 11), attitude errors were assumed to be negligible compared to navigation sensor errors.

3.6 A spherical earth was used for all geometric calculations.

3.7 Unless otherwise specified, the Andrews square-root filter was used for data processing to reduce possible roundoff errors.

3.8 A specific format for presenting the results of each system studied was used. First, a detailed description of a baseline configuration is presented in tabular form. Then results of simulating the given system are discussed. Deviations from the baseline configuration are explicitly noted and the corresponding simulation results are discussed in turn. The systems are evaluated in terms of a root-sum-squared (RSS) position error; graphical time histories of position errors are given for several key cases. Most of the data obtained, however, are summarized in tabular form.

4. UNKNOWN LANDMARK TRACKING

With an unknown landmark tracking system, satellite navigation is accomplished by making repeated measurements of the inertial direction from the satellite to a point of unknown location on the earth's surface. This so-called "unknown landmark," is visible to the satellite for only a relatively short time. After visibility is lost, another suitable unknown landmark is selected to provide additional navigation information.

This type of system has been extensively investigated in the past (Refs. 4, 5, 12, 14, 21, 22, 23, and 32). The most recent study, by Hendrickson, shows that, in spite of certain numerical problems, long term stable operation can be achieved if the data is processed with either a square root algorithm or with the usual Kalman filter using guaranteed symmetry of the covariance matrix. Hendrickson reports steady state navigation accuracies which vary between 1000 ft in the vicinity of the landmark to 3000 ft during landmark voids.

Because of the comprehensiveness of the above mentioned studies, no attempt was made in the current effort to analyze unknown landmark tracking unless it is part of a hybrid system.

However, as a check on the SNAP software, several ONAP simulations identical to those reported in the references were performed. Comparison of the results showed good agreement.

5. HORIZON SENSORS

5.1 DISCUSSION

Autonomous navigation with horizon sensors appears to be attractive for the following reasons:

a. Complete Autonomy

Other than a knowledge of inertial attitude and time, no other information is required for horizon sensors to provide complete navigation information in three dimensions.

b. Low Cost

Compared to other space navigation sensors and/or systems, the cost of horizon sensors is quite attractive since the total system only requires horizon sensors, a clock, an attitude reference system, and a computer to process the measurements.

c. Deterministic Operation

If properly used, horizon sensors can yield a deterministic position fix in three dimensions. Such information could be valuable for bootstrap initialization of more sophisticated data processing algorithms. This property can also be useful after dormant navigation periods or for recovery from possible spacecraft maneuvers.

d. Wide-Range Linear Operation

Recovery from large initial error is possible with straightforward application of usual filter algorithms because large position displacements result in only small measurement angle changes.

Unfortunately, these advantages are offset by the uncertainty in the horizon definition at any particular time. This uncertainty is a dominant error source during low-altitude operation. Currently, the lack of an adequate model for this error source is a significant limiting factor in horizon sensor navigation performance during low orbit operation.

The use of horizon sensors for navigation has received considerable attention by others (Refs. 15, 20, 24, 28, 35, and 46). The most commonly used information provided by horizon sensors is the measurement of the direction to the center of the earth. Since this measurement by itself only provides position

information in the local horizontal plane, altitude can be deduced by processing a time sequence of measurements with the known dynamical model. As a second alternative, a radar altimeter can be used to directly measure the altitude. This may not be desirable for autonomous navigation if it is preferable that the navigator be passive. A third possible choice for determining altitude involves the use of information inherently present in horizon sensor measurements. Specifically, the angle subtended by the widest apparent diameter of the earth's disk is readily computed from horizon sensor data and provides a direct approach for determining altitude. This is referred to as a planet diameter measurement in Ref. 3. If it were necessary, either the radar altimeter or the angle subtended by the earth's disk could provide deterministic position information in three dimensions when combined with the measurement of the direction to the center of the earth. Although a precise knowledge of the sensor orientation in inertial space is needed, no a priori position information is strictly required.

The geometry of horizon sensor measurements is shown in Figure 5-1. The right-handed cartesian coordinate system in Figure 5-1 is oriented such that the z_2-axis nominally points opposite to the direction of local vertical and z_1 and z_3 are in the local horizontal plane. The inability of z_2 to point exactly opposite to the local vertical direction is limited by the accuracy of the attitude control system of the vehicle and has no particular bearing on the navigation problem, providing the errors are not excessively large. Although the z-coordinate system is only coarsely aligned with the local vertical, its attitude in inertial space is assumed to be known by some precise attitude determination system such as SPARS (Refs. 10 and 11). Hence, the attitude errors are assumed to be negligible compared to the errors in the horizon sensor.

The measurement of the direction to the center of the earth is defined by two angles θ_1 and θ_1' which are shown in Figure 5-2a. These angles can by expressed in terms of the ECI (see Appendix C) vehicle position coordinates, x_1, x_2, x_3 as:

$$\theta_1 = \arccos\left[s_3 / \left(s_2^2 + s_3^2\right)^{1/2}\right] \qquad (5\text{-}1)$$

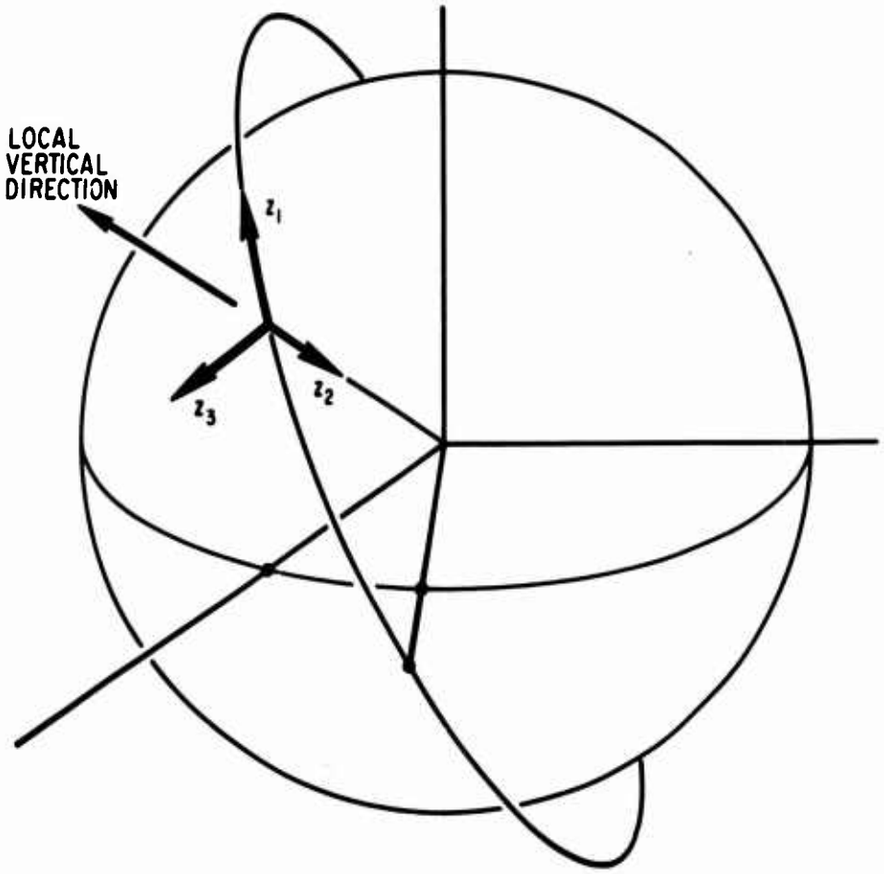

Figure 5-1. Horizon Sensor Coordinate System

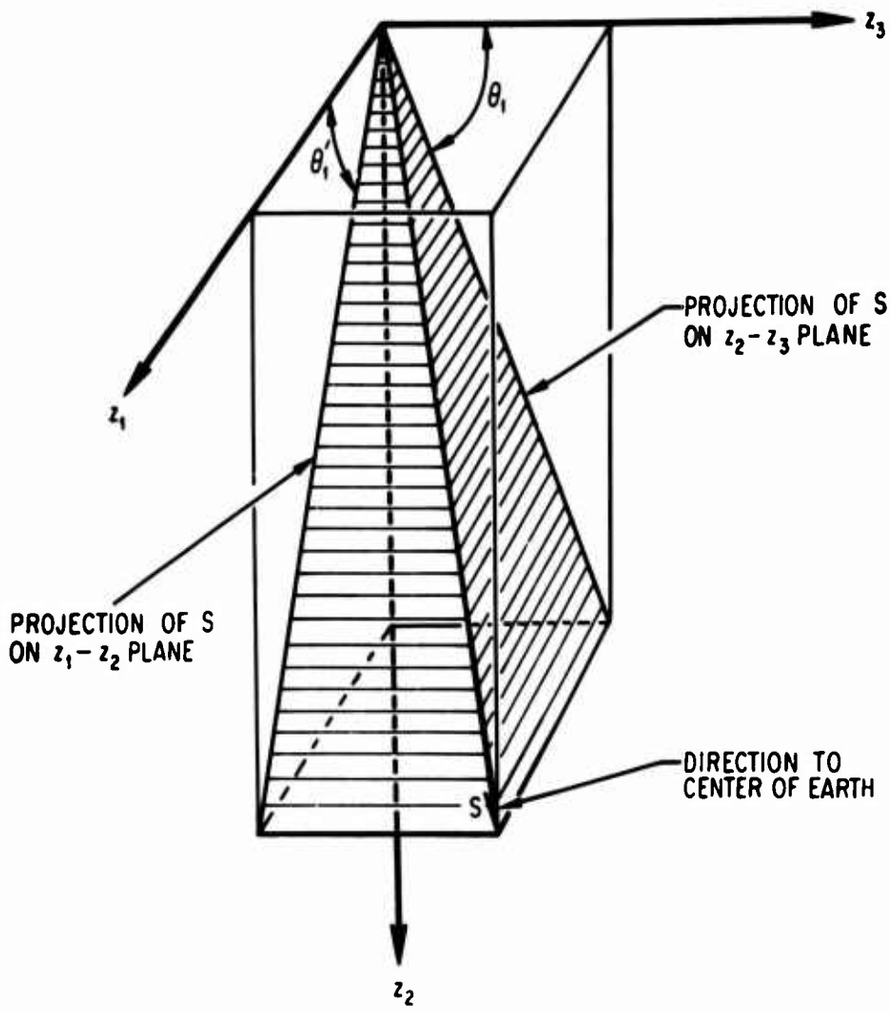

Figure 5-2a. Horizon Sensor Measurement Geometry

$$\theta_1' = \arccos\left[s_1 / \left(s_1^2 + s_2^2\right)^{1/2}\right] \tag{5-2}$$

where

$$\begin{bmatrix} s_1 \\ s_2 \\ s_3 \end{bmatrix} = -B \begin{bmatrix} x_1 \\ x_2 \\ x_3 \end{bmatrix} \tag{5-3}$$

and the rotation matrix B is known from the assumed attitude reference system. Figure 5-2b has been drawn to emphasize the angle definitions. In reality, θ_1 and θ_1' should be very close to 90 deg if the attitude control system is performing properly. The angle subtended by the widest diameter of the earth's apparent disk is defined to be θ_2 and is shown in Figure 5-2b; θ_2 can be expressed as

$$\theta_2 = 2 \arcsin\left[R_e/(R_e + h)\right] \tag{5-4}$$

where R_e is the radius of the earth and h is the altitude of the navigator.

These measurements are corrupted by both sensor noise and horizon definition errors. The former is due to the inability of the sensor to perfectly discern the 14 - 16 μ CO_2 absorption layer (the phenomena detected by high performance sensors such as Quantic Mod IV) (Ref. 46). The magnitude of this error is on the order of 0.01 deg (1σ) and is assumed to be white noise in this study. The dominant error source, however, is not in the sensors themselves, but in the uncertainty of the altitude of the CO_2 absorption layer. It can be shown that these horizon errors are time- and space-correlated (Refs. 16 and 34). Thus they can be modeled as Markov processes (Ref. 28). The derivation of the appropriate relationships describing the effect of these

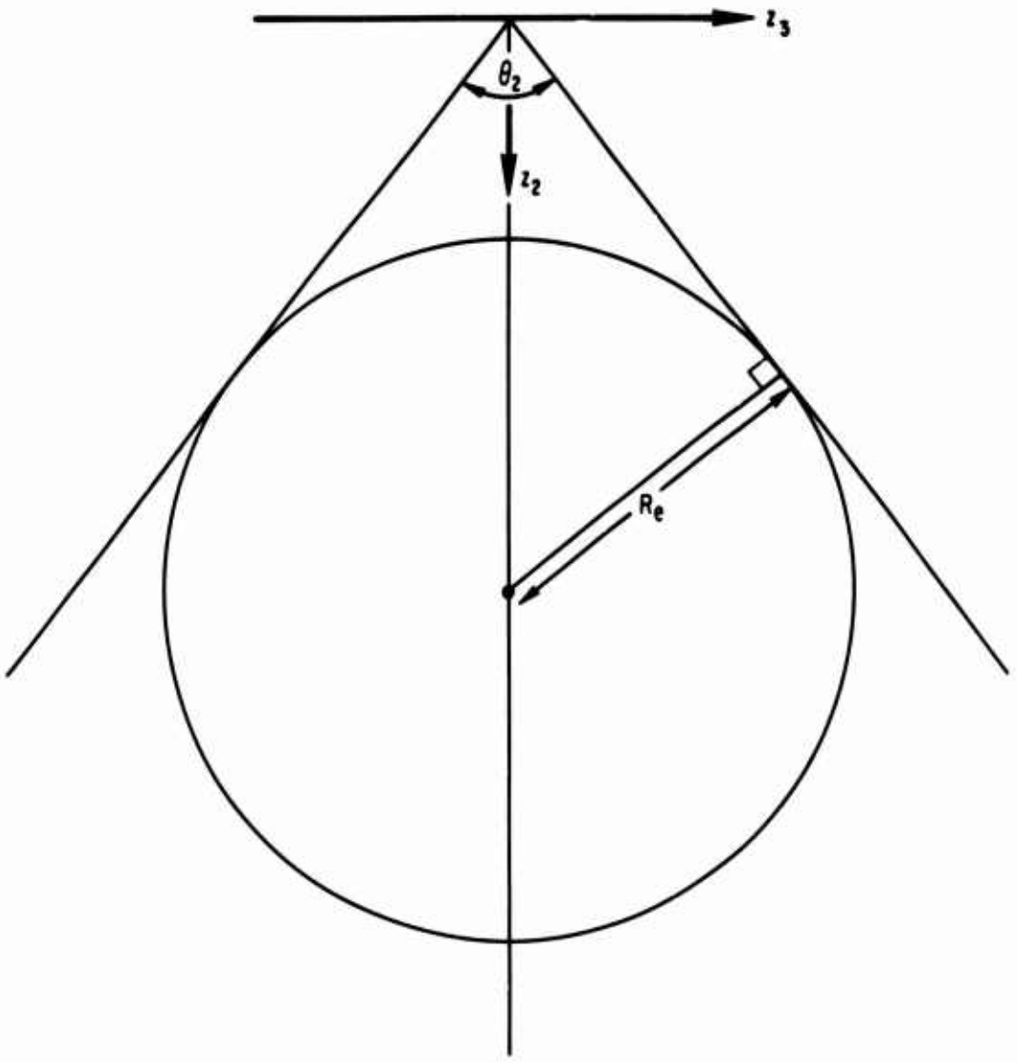

Figure 5-2b. Angle Subtended by Disk of Earth

errors on the observations is somewhat involved and only the key results are given here. It is shown in Appendix D that the horizon errors in θ_1, θ_1', and θ_2, represented by the state variables x_7, x_8, x_9, respectively, propagate in time according to the differential equations

$$\begin{aligned} \dot{x}_7 &= -x_7/625 + u_7 \\ \dot{x}_8 &= -x_8/625 + u_8 \\ \dot{x}_9 &= -x_9/625 + u_9 \end{aligned} \tag{5-5}$$

where

$$\begin{aligned} \mathcal{E}\left[x_7^2(0)\right] &= 0.01485^2 \text{ deg}^2 \\ \mathcal{E}\left[x_8^2(0)\right] &= 0.01485^2 \text{ deg}^2 \\ \mathcal{E}\left[x_9^2(0)\right] &= 0.05145^2 \text{ deg}^2 \end{aligned} \tag{5-6}$$

and u_7, u_8, and u_9 are white noise defined by

$$\begin{aligned} \mathcal{E}[u_7(t)u_7(\tau)] &= 7.05 \times 10^{-7}\delta(t-\tau) \text{ deg}^2/\text{sec}^2 \\ \mathcal{E}[u_8(t)u_8(\tau)] &= 7.05 \times 10^{-7}\delta(t-\tau) \text{ deg}^2/\text{sec}^2 \\ \mathcal{E}[u_9(t)u_9(\tau)] &= 8.47 \times 10^{-6}\delta(t-\tau) \text{ deg}^2/\text{sec}^2 \end{aligned} \tag{5-7}$$

5.2 BASELINE CONFIGURATION AND ASSOCIATED RESULTS

The system discussed in Sect. 5.1 was analyzed in a series of simulations. The baseline configuration is described in Table 5-1.

Table 5-1. Baseline Horizon Sensor Configuration

Key Parameters

Measurement Model	1. Angle subtended by disk of earth 2. Two angles to apparent center of earth
Gravity Model	Real World: APL "8-8" Filter World: μ and J_2
Atmosphere Model	Real World: U.S. Standard 1962 Filter World: Exponential
Data Rate	1 Sample/30 sec
Measurement Noise and Biases	0.01 deg (1σ) random noise Markov biases (see Sect. 5.1)
Forcing Noise	None except for noise on Markov processes (see Eqs. (5-5), (5-6), (5-7))

Initial Conditions

States	Real World	Filter World (all states estimated)	Standard Deviation
x_1, x_2, x_3 (inertial position)	Reference Orbit	6700 ft offset (in each direction)	10000 ft
x_4, x_5, x_6 (inertial velocity)	Reference Orbit	6.7 ft/sec offset (in each direction)	10 ft/sec
x_7, x_8 (Markov biases)	0 deg	0.01485 deg	0.01485 deg
x_9 (Markov bias)	0 deg	0.05145 deg	0.05145 deg

5.2.1 The results of simulating the baseline configuration are shown graphically in Figure 5-3 and are indicated below. After about one-half orbit the steady state condition is reached. The position standard deviations converge to

1400 ft Radial
4500 ft Intrack
2800 ft Crosstrack
5500 ft RSS

5.2.2 Model errors do not appear to have an effect until the second orbit.

5.2.3 The Markov biases in the sensor measurements are weakly observable. The standard deviations of the bias in the angles defining the direction to the center of the earth were reduced to 2/3 of their a priori values after half an orbit, while the standard deviation for the bias in the angle subtended by the earth's disk was reduced by 1/2 in that same time interval.

5.2.4 The basic performance of the horizon sensor is limited by the error model used for the altitude of the CO_2 absorption layer.

5.3 INITIAL CONVERGENCE ANALYSIS

5.3.1 The baseline case was compared to cases with initial position errors and corresponding standard deviations of 5, 10, and 20 miles. Table 5-2 gives the position errors obtained after the angle subtended by the earth disk and two angles defining the direction to the center of the earth have been processed by the filter. The agreement between the state residuals and the corresponding standard deviations indicates that a linear algorithm is sufficient for initialization for position offset as large as 20 miles. With errors this large, the effect of the a priori covariance is negligible. Thus a deterministic solution should give comparable errors.

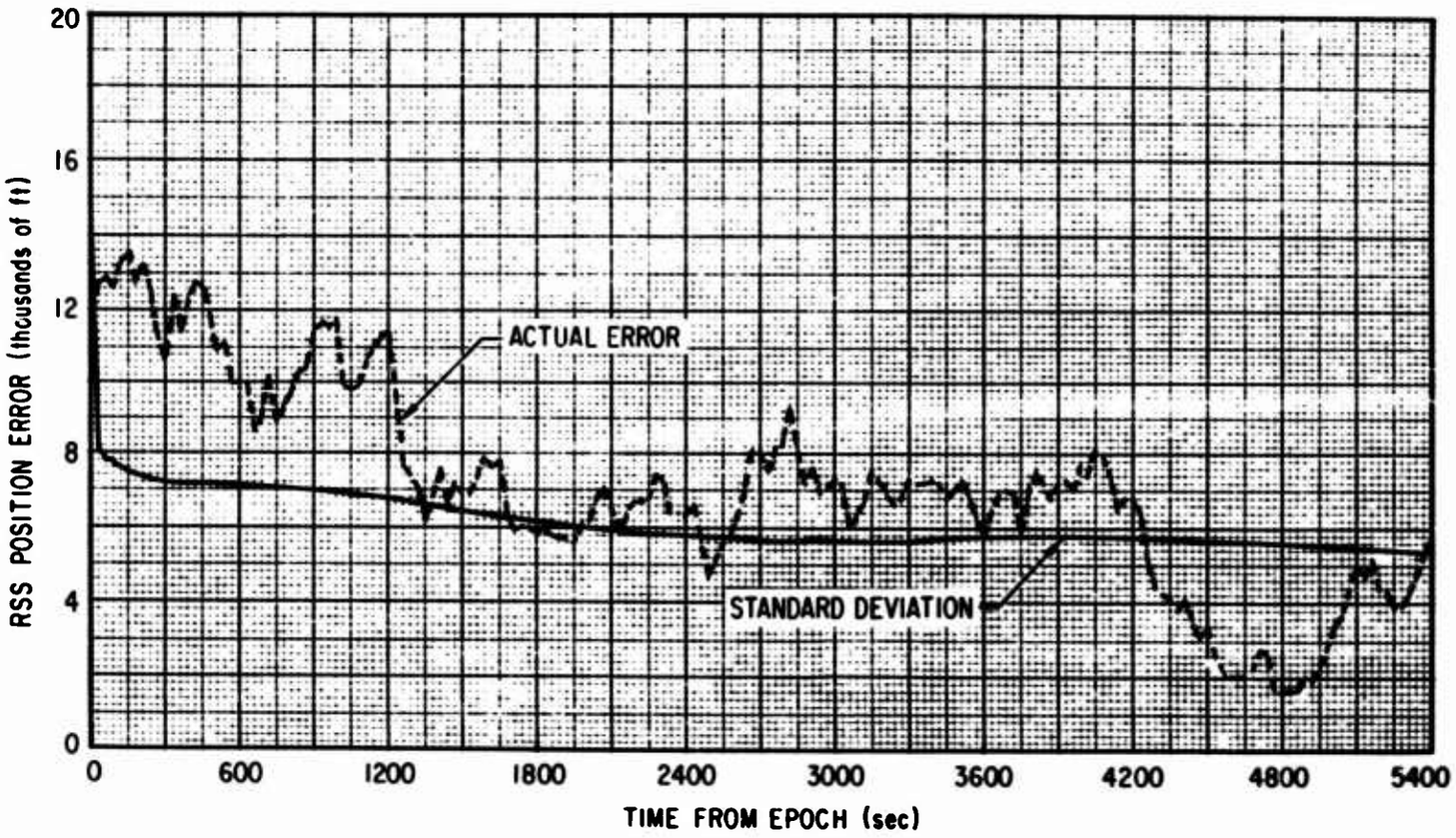

Figure 5-3. RSS Position Errors for Baseline Horizon Sensor System

Table 5-2. Errors Obtained after One Set of Horizon Sensor Measurements

Initial Position Errors (n mi)	Radial		Intrack		Crosstrack		RSS	
	State Residual (ft)	Standard Deviation (ft)	State Residual (ft)	Standard Deviation (ft)	State Residual (ft)	Standard Deviation (ft)	State Residual (ft)	Standard Deviation (ft)
1	-3004.	3100	-974.	5600	-6114.	5600	6882.	8607
5	-2500.	3300	-5104.	6800	-6314.	6800	8496	10212
10	-1625.	3400	-4717.	6900	-5945.	6900	7762	10311
20	1699.	3500	-3960.	6900	-5197.	6900	6752	10394

5.3.2 Convergence to the values given in Sect. 5.2.1 occurs in about 1/2 orbit and is apparently independent of the magnitude of the initial errors for the particular orbit studied.

5.3.3 Removal of the information provided by the measurement of the angle subtended by the earth's disk resulted in a delay of convergence until the end of the first orbit. Furthermore, such a system does not provide the capability for deterministic operation.

5.3.4 Although the accuracy attainable with horizon sensors is limited, the advantages gained by their convergence properties suggest their use as auxiliary sensors in a general autonomous navigation system.

6. UNKNOWN LANDMARK TRACKER WITH HORIZON SENSORS

Upon examining the results on both unknown landmark tracking and horizon sensors, it is natural to consider a hybrid configuration containing both sensors. The properties of these sensors certainly appear to complement each other quite well. Accurate navigation information could be supplied by the unknown landmark tracker while initialization and error bounding during landmark voids could easily be accommodated by the horizon sensor. In addition, both sensors are highly autonomous.

6.1 BASELINE CONFIGURATION AND ASSOCIATED RESULTS

The baseline configuration used is described in detail in Table 6-1.

6.1.1 The results obtained by simulating the baseline case are indicated graphically in Figure 6-1 and summarized in Table 6-2. Although the performance is about three times better than with the horizon sensor alone, the system does not appear capable of producing accuracies much better than 2000 ft.

6.1.2 Removal of the horizon sensors from the baseline configuration yields the results shown in Figure 6-2 and Table 6-3. Comparison of Tables 6-2 and 6-3 shows how valuable horizon sensors can be for initialization and for bounding error growth during landmark voids.

6.2 EFFECT OF INCREASED LANDMARK VISIBILITY TIME

As a possible improvement to the baseline performance, the line of sight-nadir angle was increased from 45 to 60 deg to allow longer visibility times for each landmark. Atmospheric refraction was ignored to simplify the analysis. A comparison of the results displayed in Table 6-4 with those of Table 6-2 shows the effect is relatively marginal. Indeed, since the hardware problem associated with landmark definition near the horizon is quite formidable, there is little reason to consider the approach any further.

Table 6-1. Baseline Unknown Landmark Tracker-Horizon Sensor Configuration

Key Parameters

Measurement Set	1. Two angles to an unknown landmark. 2. Two angles to the apparent center of the earth (bisector angles). 3. Angle subtended by earth's disk
Gravity Model	Real World: APL 8-8 Filter World: μ and J_2
Atmosphere Model	Real World: U.S. Standard 1962 Filter World: exponential
Data Rate	Unknown landmark tracker: Landmarks were "generated" in the orbit plane 45 deg from nadir at 120, 450, 1140, 1620, 3360, and 3900 sec from epoch. Observations were taken every 10 sec until the line of sight to the landmark was more than 45 deg from nadir. Horizon sensors: 1 sample 30/sec (continuously)
Measurement Noise and Biases	Unknown landmark tracker: 10 arc sec random (1σ), 30 arc sec bias Horizon sensor: 0.01 degree random (1σ) Markov biases (see Sect. 5.1)
Forcing Noise	None except for Markov biases.

Initial Conditions

States	Real World	Filter World (all states estimated)	Standard Deviation
x_1, x_2, x_3 (Inertial position)	Reference Orbit	6700 ft offset in each direction	10,000 ft
x_4, x_5, x_6 (Inertial velocity)	Reference Orbit	6.7 ft/sec offset in each direction	10 ft/sec
x_7, x_8 (Markov biases)	0 deg	0.01485 deg	0.01485 deg
x_9 (Markov bias)	0 deg	0.05145 deg	0.05145 deg
x_{10}, x_{11} (Landmark latitude, longitude)	Computed	Computed	Computed
x_{12} (Landmark altitude)	3000 ft	Random offset 1500 ft (1σ)	1500 ft (1σ)
x_{13}, x_{14} (Landmark angle biases)	0 deg	0.0083 deg	0.0083 deg

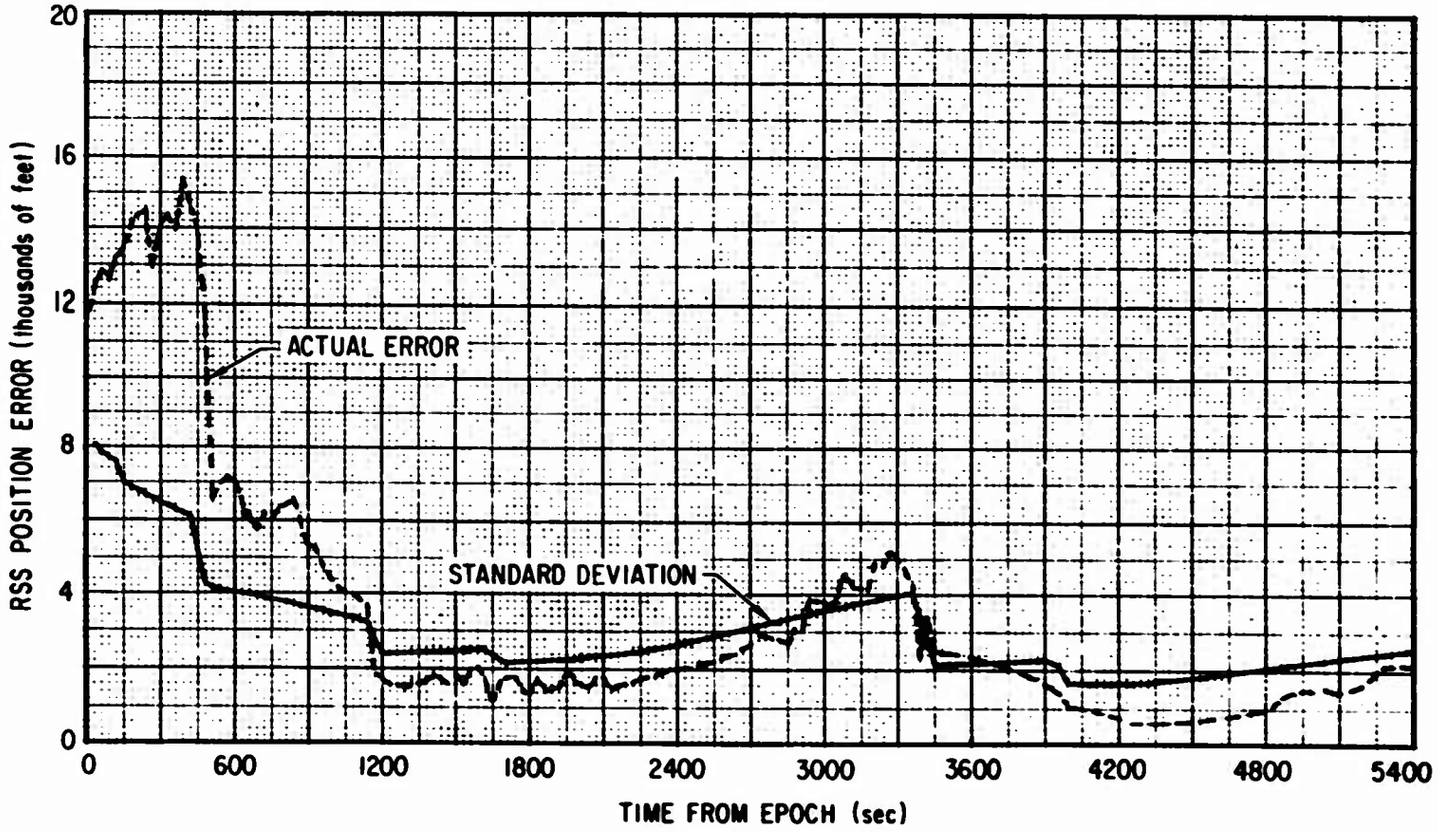

Figure 6-1. RSS Position Errors for Baseline Unknown Landmark Tracker - Horizon Sensor System

Table 6-2. RSS Position Error for Baseline Unknown Landmark Tracker-Horizon Sensor

Time of Acquisition and Termination of Landmark (sec)	Landmark Number	RSS Error (ft)	RSS Standard Deviation (ft)
0	-	11,640	17,321
120	1	13,230	7,570
210		14,391	6,722
450	2	13,914	6,006
540		6,893	4,195
1140	3	3,682	3.251
1200		1,822	2,437
1620	4	1,701	2,586
1680		1,309	2,184
3360	5	4,356	4,038
3450		2,546	2,143
3900	6	1,614	2,295
4020		1,124	1,663
5400	-	2,123	2,560

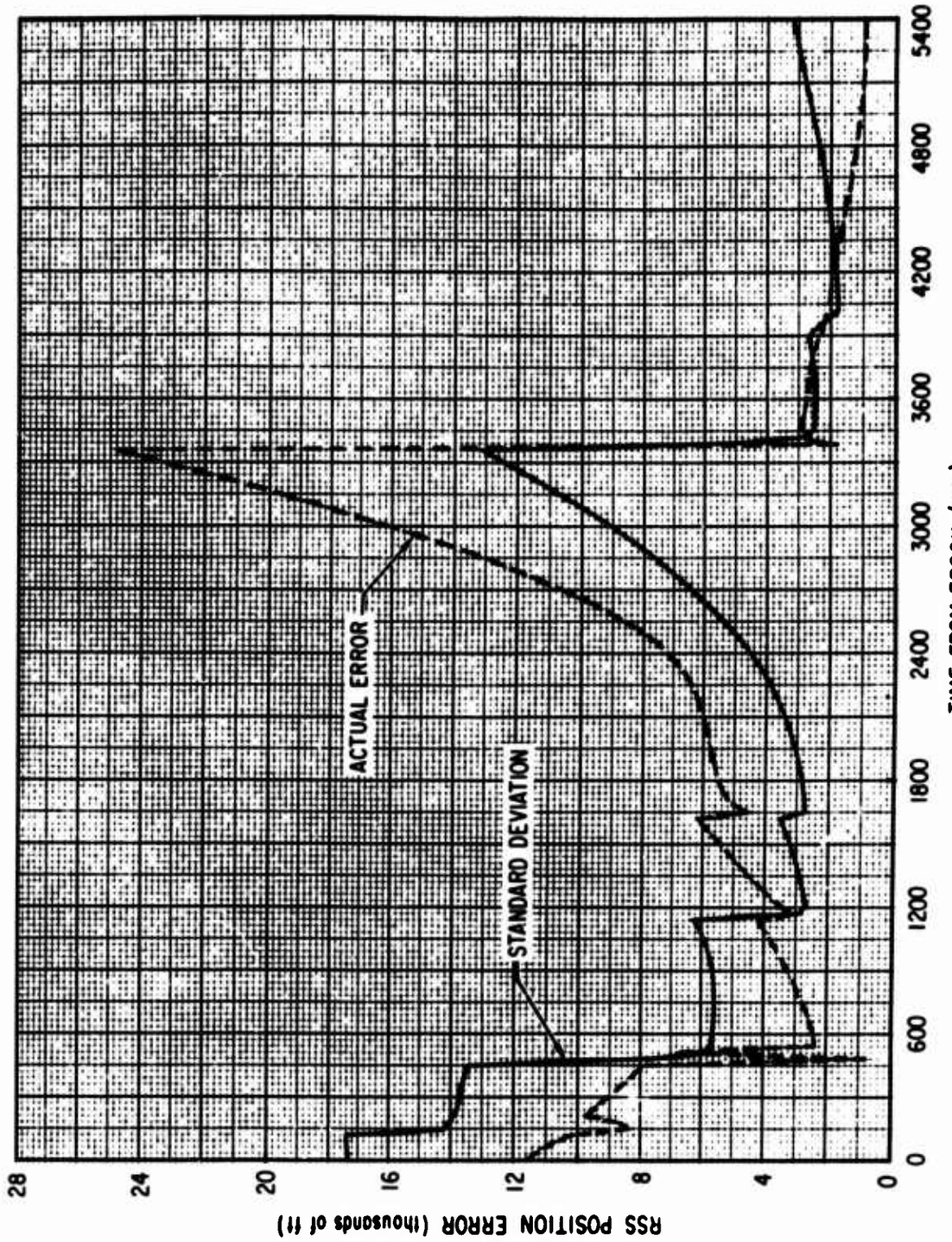

Figure 6-2. RSS Position Errors for Unknown Landmark Tracker

Table 6-3. RSS Position Error for Baseline Unknown Landmark Tracker without Horizon Sensor

Time of Acquisition and Termination of Landmark (sec)	Landmark Number	RSS Error (ft)	RSS Standard Deviation (ft)
0	-	11,640	17,321
120	1	10,204	17,446
210		9,748	13,888
450	2	7,851	13,448
540		2,392	5,656
1140	3	4,201	6,291
1200		3,503	2,732
1620	4	6,181	3,539
1680		5,190	2,699
3360	5	24,814	13,115
3450		2,911	2,452
3900	6	2,431	2,647
4020		2,096	1,817
5400	-	972	3,178

Table 6-4. Effect of 60 Deg Maximum Line of Sight-Nadir Angle on Unknown Landmark Tracker-Horizon Sensor RSS Position Error

Time of Acquisition and Termination of Landmark (sec)	Landmark Number	RSS Error (ft)	RSS Standard Deviation (ft)
0	-	11,604	17,321
120 210*	1	13,230 14,319	7,570 6,766
450 540*	2	12,293 5,871	5,884 3,853
1140 1200*	3	2,950 1,322	2,823 2,117
1620 1680*	4	1,567 706	2,225 1,903
3360 3450*	5	2,429 1,661	3,650 1,719
3900 4020*	6	1,591 2,092	1,538 1,285
5400	-	1,459	2,082

*These entries are <u>not</u> landmark termination times.

6.3 EFFECT OF LANDMARK DENSITY

6.3.1 In order to determine the effect of increasing the landmark density, several two-orbit computer runs were made. First, the baseline simulation was extended to the end of the second orbit; then, a similar configuration with twelve more or less uniformly distributed landmarks per orbit was simulated; and, finally, the hypothetical situation of unlimited landmark availability was considered. In all cases, the actual RSS error became meaningless in the second orbit because of uncompensated model errors. Thus only the RSS standard deviations were reported. The results, displayed in Table 6-5, represent a lower bound since the effect of model error is not included.

6.3.2 Basically, the results show that a major increase in landmark density is required to bring about a significant decrease in error. It is doubtful that a sufficient increase in landmarks could be obtained in practical situations to warrant the effort.

6.4 EFFECT OF LANDMARK DISTRIBUTION

The baseline landmark acquisition schedule chosen did not allow for possible voids due to operation over cloud-covered or night areas. In Refs. 5, 12, and 16, the day-night problem was considered using five landmarks per orbit, all concentrated on the "day" side. The results reported showed oscillations in accuracy from 1000 to 3000 ft. As shown in Table 6-5, use of a similar number of landmarks distributed more evenly prevents such large variations with very little degradation in maximum attainable accuracy. Thus, landmark distribution is critical for bounding errors, but is not very effective for improving the navigation accuracy.

6.5 USE OF LANDMARKS WITH KNOWN ALTITUDES

6.5.1 If landmarks were restricted to the coastline, the uncertainty in landmark altitude would become extremely small. The effect is essentially equivalent to the removal of landmark altitude from the state vector. The

Table 6-5. Effect of Landmark Density on Unknown Landmark Tracker-Horizon Sensor RSS Position Error

Time from Epoch (sec)	RSS Standard Deviation for Baseline Configuration (6 landmarks per orbit) (ft)	RSS Standard Deviation (12 landmarks per orbit) (ft)	RSS Standard Deviation with Unlimited Landmark Availability (66 landmarks per orbit) (ft)
0	17,321	17,321	17,321
1,000	3,470	3,000	1,650
2,000	2,300	2,050	977
3,000	3,572	2,356	809
4,000	1,662	1,413	792
5,000	2,240	1,360	670
6,000	2,815	1,539	621
7,000	1,980	1,250	559
8,000	1,565	1,140	462
9,000	1,470	1,119	465
10,000	1,104	922	439

results obtained from simulating such a situation are sumarized in Table 6-6. Comparison with Table 6-2 shows that a 50 percent improvement can be obtained by the suggested technique.

6.5.2 As might be expected, the use of landmarks with known altitudes reduces the radial error drastically. An order of magnitude reduction in this error was observed.

6.6 PERFORMANCE WITH A HIGH ACCURACY SENSOR

6.6.1 In order to assess the "ultimate" performance of an unknown landmark tracker, a high accuracy sensor with 2 arc sec of random noise (1σ) and 4 arc sec of bias was considered. The results of using this configuration are shown in Column A of Table 6-7. While the errors are considerably less than those observed for the baseline case, they were not significantly different from those using the baseline sensor with coastline landmarks.

6.6.2 The effect of assuming coastline landmark with the high accuracy sensors is shown in Column B of Table 6-7. A considerable improvement in performance of the error analysis is clearly obtained. Note, however, that model errors now become quite significant by the end of the first orbit.

6.6.3 The effect of removal of both atmosphere and geopotential model errors is shown in Column C of Table 6-7. These results indicate that improved geopotential models and the possible use of accelerometers for drag measurement could provide a significant increase in accuracy.

6.6.4 It should be noted that although high accuracy navigation with unknown landmark trackers is indicated by these results, the underlying assumptions are not realistic. The feasibility of building a sensor with the required accuracy and the ability to distinguish coastlines from other landmarks has, by no means, been demonstrated. Furthermore, the results obtained were

Table 6-6. RSS Position Errors for Baseline Unknown Landmark Tracker and Horizon Sensor with Coastline Landmarks

Time of Acquisition and Termination of Landmark (sec)	Landmark Number	RSS Error (ft)	RSS Standard Deviation (ft)
0	-	11,640	1732
120 210	1	13,230 14,646	7570 6638
450 540	2	13,677 5,475	5834 2856
1140 1200	3	3,729 1,530	2738 1320
1620 1680	4	119 328	1095 974
3360 3450	5	2,574 1,937	1349 1189
3900 4020	6	1,192 763	1047 914
5400	-	2,061	964

Table 6-7. RSS Position Errors for Unknown Landmark Tracker-Horizon System with High Accuracy Sensor

Time of Acquisition and Termination of Landmark (sec)	A High Accuracy Sensor Only		B High Accuracy Sensor with Coastline Landmarks		C High Accuracy Sensor, Coastline Landmarks, No Model Error
	RSS Error (ft)	RSS Standard Deviation (ft)	RSS Error (ft)	RSS Standard Deviation (ft)	RSS Error (Standard Deviation same as B) (ft)
0	11,605	17,321	11,605	17,321	11,605
120	13,230	7,570	12,318	7,569	12,321
210	14,164	6,471	13,588	6,333	13,569
450	13,211	5,743	11,778	5,544	11,815
540	3,819	3,057	1,055	688	1,129
114[illegible]	1,231	2,498	823	1,007	782
1200	974	1,460	529	267	375
1620	1,192	1,752	344	225	117
1680	1,707	1,302	307	196	104
3360	1,011	3,220	1,068	298	454
3450	744	920	932	238	402
3900	669	975	794	213	297
4020	592	613	637	185	220
5400	722	1,429	716	194	267

based on a relatively uniform landmark distribution, whereas a real system must allow for sizable landmark voids during operation at night or under conditions with heavy cloud cover.

7. RANGE RATE TO KNOWN GROUND STATIONS

Although the configuration considered in the previous section was highly autonomous, certain rather optimistic assumptions were required to obtain high accuracy navigation performance. In an attempt to meet such a goal more realistically, the autonomy requirement was relaxed and navigation by means of range rate to known ground stations was considered.

7.1 BASELINE CONFIGURATION AND ASSOCIATED RESULTS

The baseline configuration described in Table 7-1 used 21 ground stations which were chosen at locations near existing doppler installations. The assumed coordinates are given in Appendix F.

7.1.1 The ground trace of the first orbit for the reference ephemeris of Appendix C is shown in Fig. 7-1. Those ground stations visible to the satellite are also indicated on that diagram.

7.1.2 The time history of the RSS position errors for the baseline case is shown graphically in Figure 7-2. The results before and after acquisition of each ground station are summarized in Table 7-2. Although the errors decrease after each ground station acquisition, they grow quite rapidly when no measurements are taken. By the second orbit, however, this pattern of wild error fluctuation appears to stabilize.

7.1.3 Unmodeled dynamic errors do not become significant until well into the second orbit.

7.2 EFFECT OF INCREASING NUMBER OF GROUND STATIONS

7.2.1 It was hypothesized that the relative instability noted in the first orbit of the baseline case can be attributed to an insufficient number of ground station acquisitions. In order to test this hypothesis, additional stations were assumed. In choosing the locations, an attempt was made to provide as

Table 7-1. Baseline Configuration for Range Rate to Known Ground Stations

Key Parameters

Measurement Model	Instantaneous range rate
Number of Stations	21
Gravity Model	Real World: 8-8 Filter World: μ and J_2
Atmosphere Model	Real World: U.S. Standard 1962 Filter World: exponential
Data Rate	1 sample/10 sec
Measurement Noise	1.67 ft/sec (1σ)
Forcing Noise	None
Minimum Elevation Angle for ground station visibility	5 deg

Initial Conditions

State	Real World	Filter World (all states estimated)	Standard Deviation
x_1, x_2, x_3 (inertial position)	Reference Orbit	6700 ft offset (in each direction)	10,000 ft/sec
x_4, x_5, x_6 (inertial velocity)	Reference Orbit	6.7 ft/sec offset (in each direction)	10 ft/sec

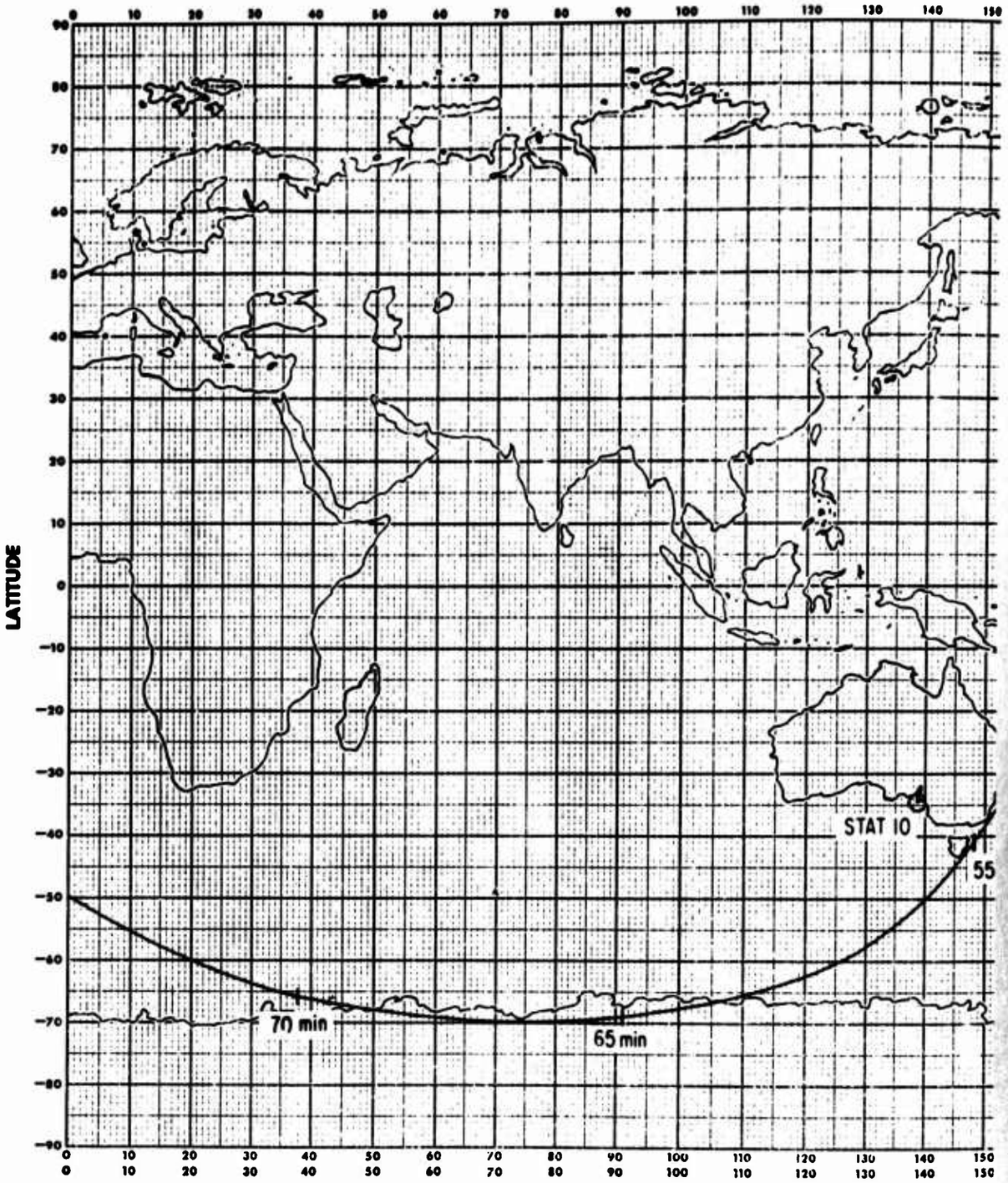
LATITUDE
STAT 10
55
70 min
65 min

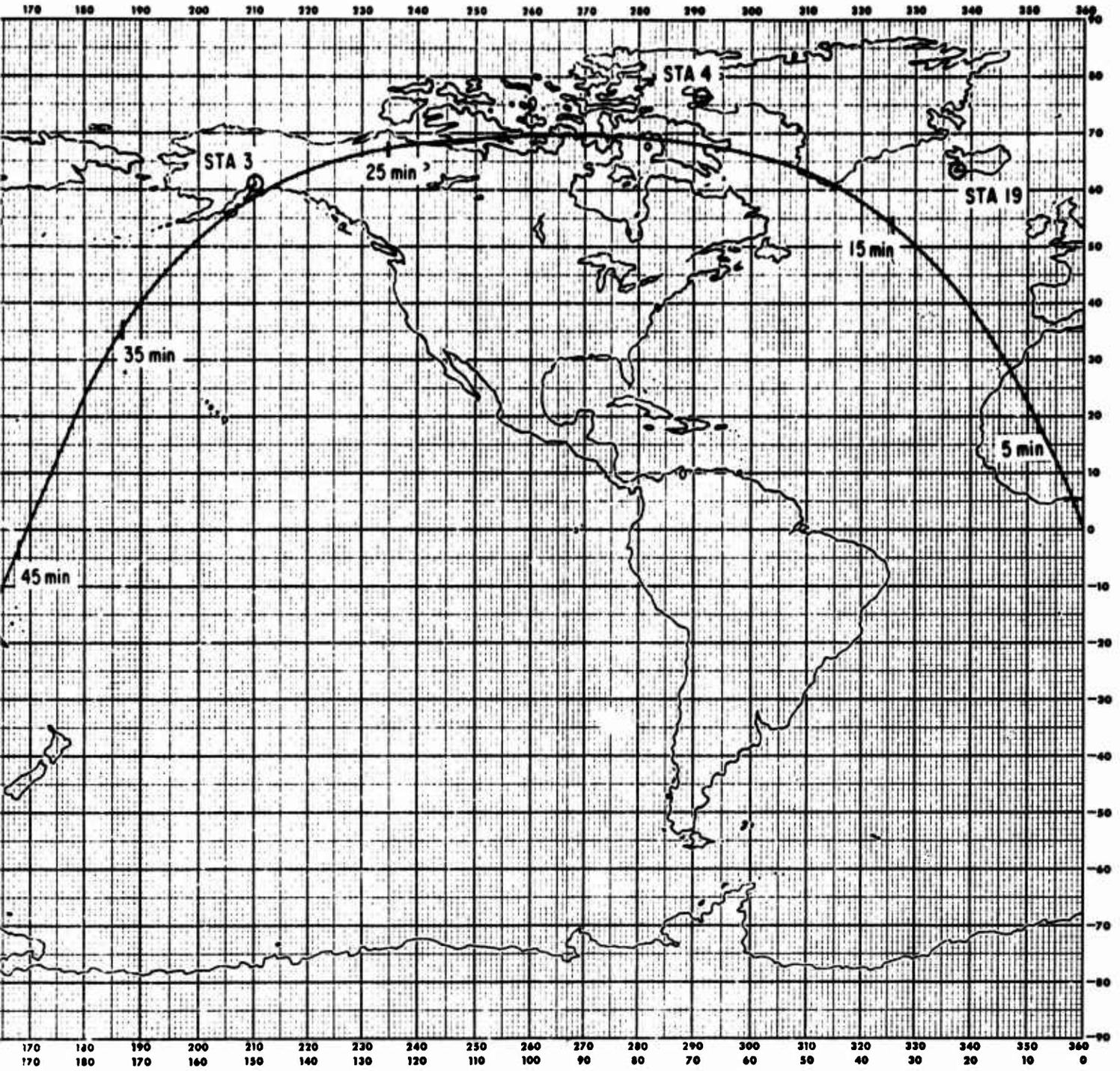

Figure 7-1. First Orbit Ground Trace Showing Visible Stations (21 ground station system)

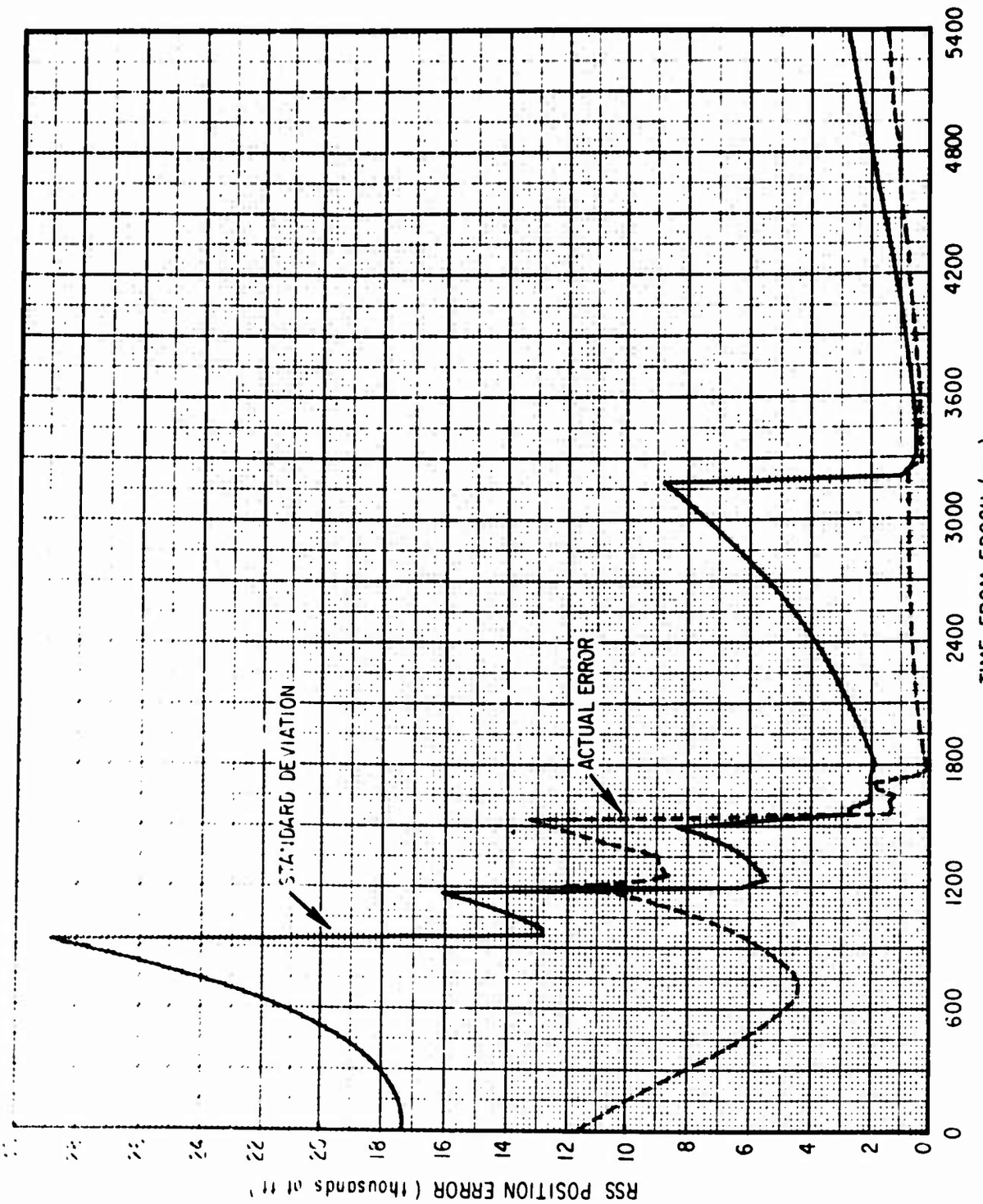

Figure 7-2. RSS Position Errors for Baseline Range-Rate System

Preceding page blank

Table 7-2. RSS Position Errors for Baseline Range Rate Configuration

Time of Acquisition and Termination of Ground Station (sec)	Station Number	RSS Error (ft)	RSS Standard Deviation (ft)
0	--	11605	17321
930 990	19	6045 6502	28938 12772
1170 1320	4	10159 8788	16092 5665
1590 1800	3	13307 144	8759 1865
3180 3390	10	715 299	8824 469
5400	--	1473	2798

near worldwide coverage as possible, without, of course, utilizing any politically excluded territory. Island installations were used extensively to avoid large gaps in ocean coverage. The final list contains 104 stations, including the 21 used for the baseline case (see Appendix F). The coordinates of stations 22 through 104 were rounded to the nearest 5 deg to facilitate program input and graphical work. The first orbit ground trace with the associated visible stations using the complete list is shown in Figure 7-3.

7.2.2 The results of a range rate navigation simulation with the 104 station deployment are displayed graphically in Figure 7-4. As anticipated, error osillations are drastically reduced and a low steady state error is reached quite rapidly in about one-third of an orbit. However, because of the improved accuracy, model errors become noticeable during the first orbit.

7.3 INITIAL CONVERGENCE ANALYSIS

Cases with initial position offsets of 5 and 10 n mi with 104 ground stations were studied in order to determine the convergence properties of the assumed measurement configuration. The results, which are summarized in Table 7-3, show that filter convergence with initial errors of 5 n mi or more cannot be obtained. This suggests possible augmentation of the range rate configuration with horizon sensors.

7.4 RANGE RATE WITH ANGLE SUBTENDED BY EARTH'S DISK

7.4.1 Since range rate observations do not require precise vehicle attitude information, it would be desirable that any sensor introduced for improving convergence properties should also be independent of such information. While the complete horizon sensor system described in Section 5 implicitly requires a precise attitude reference system, the angle subtended by the earth's disk does not, and could conceivably be used to augment the range rate measurement. This contention was tested in a series of simulations in which the initial position offset was varied. The results are summarized in Table 7-4.

7.4.2 Comparison of Tables 7-4 and 7-2 shows that, while the angle subtended by the earth's disk prevents catastrophic failures, it by no means provides an adequate solution to the convergence problem.

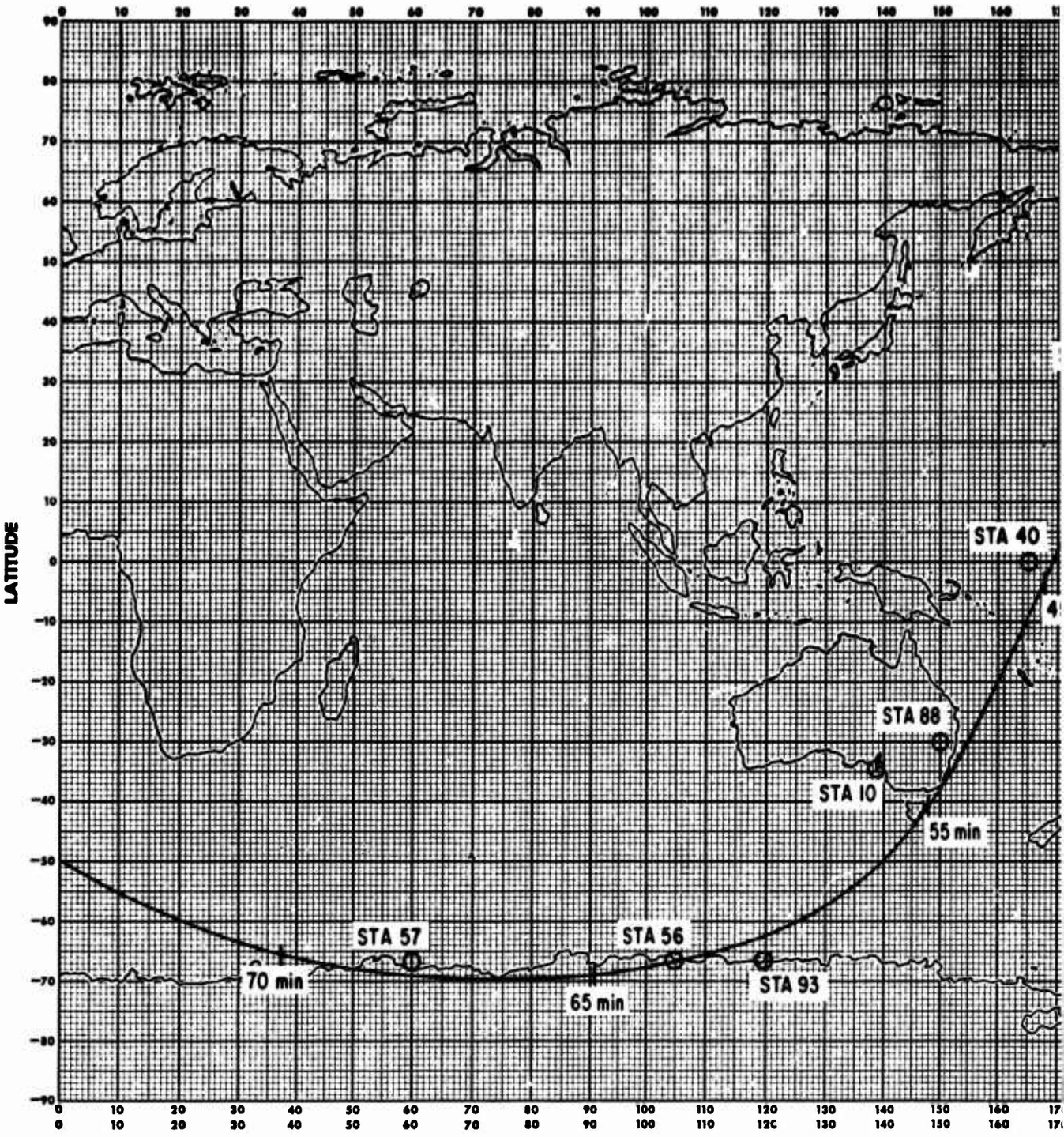
LATITUDE
STA 40
STA 88
STA 10
55 min
STA 57
STA 56
70 min
65 min
STA 93

9a

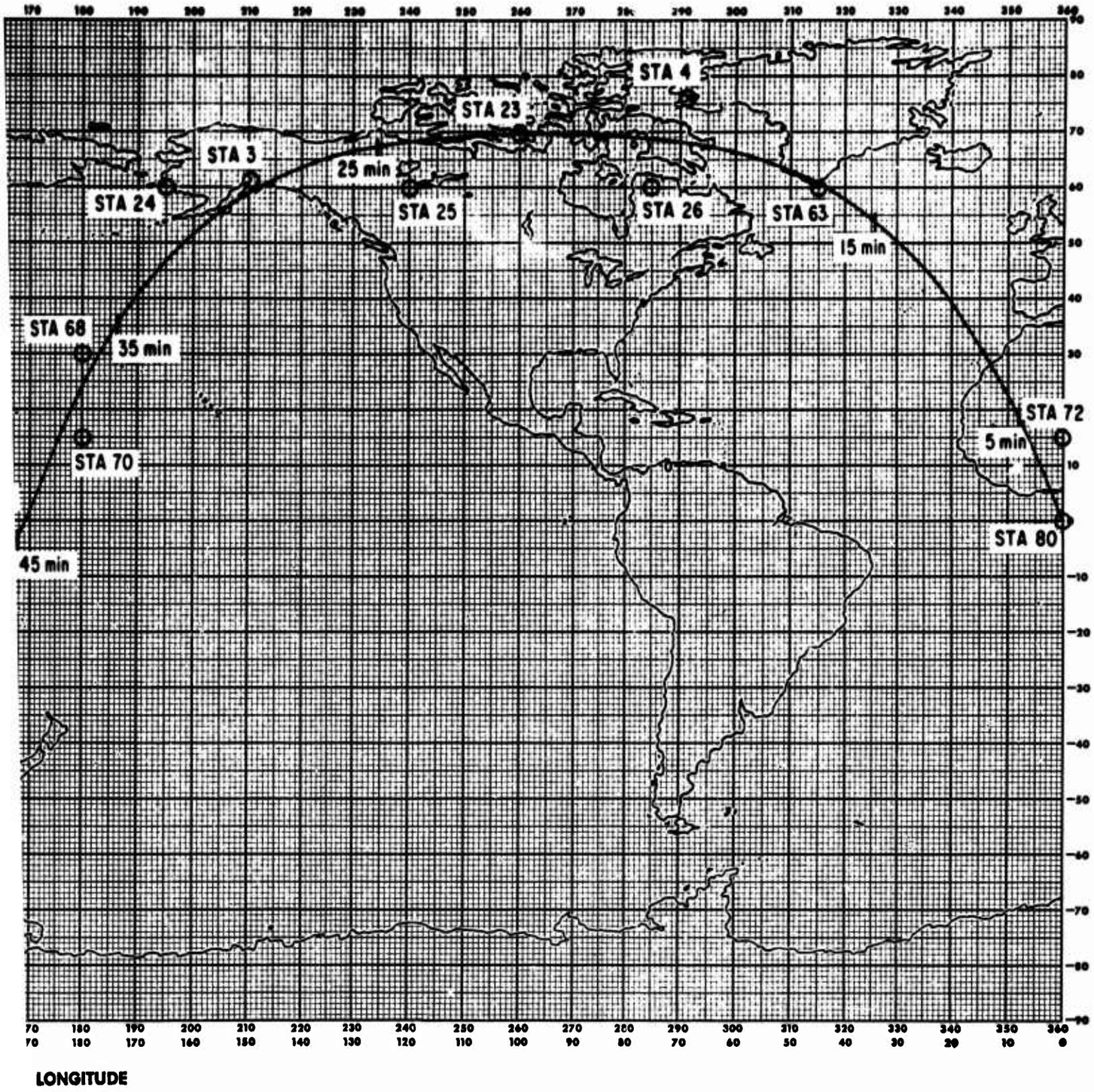

Figure 7-3. First Orbit Ground Trace Showing Visible Stations (104 ground station system)

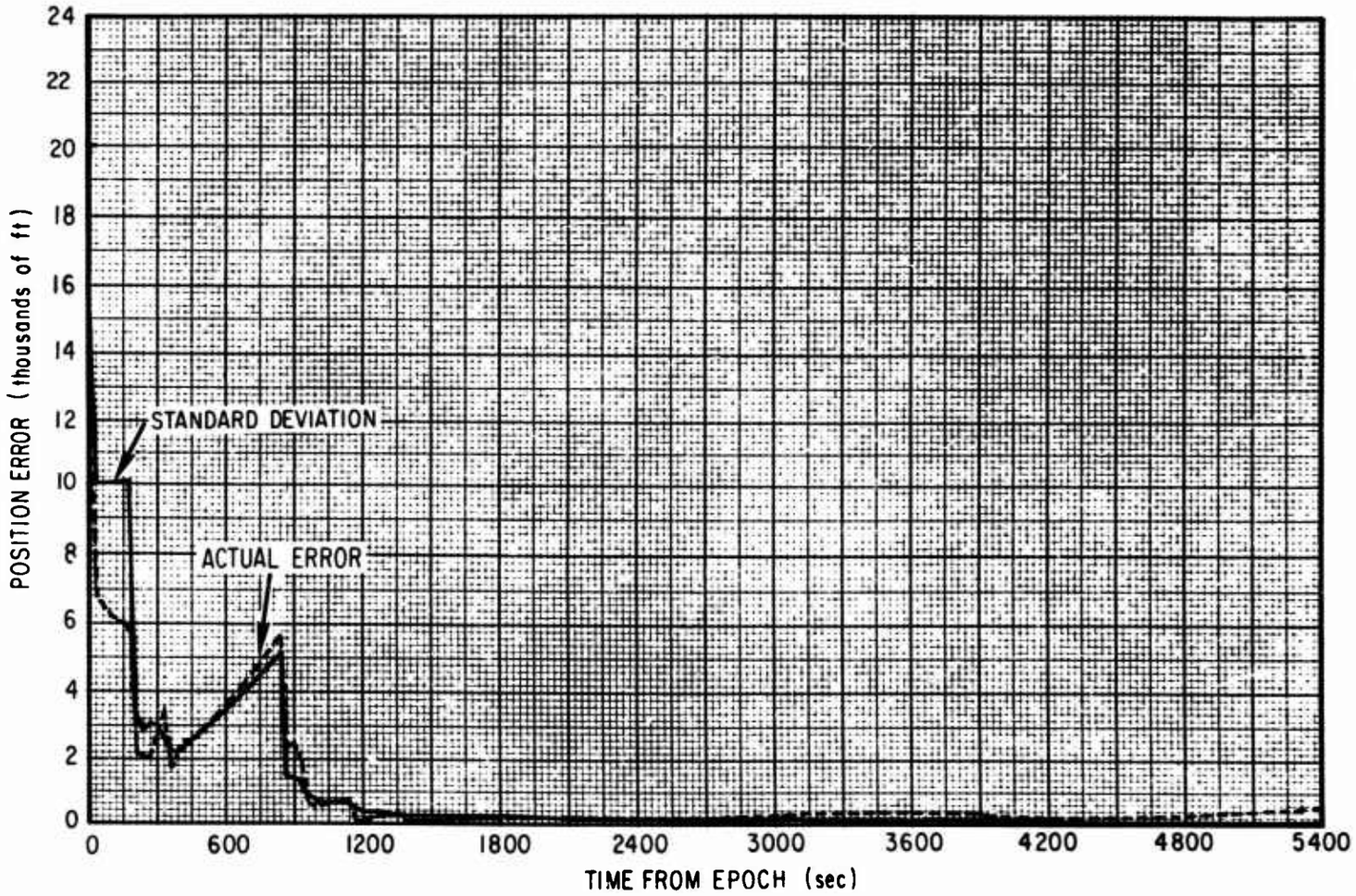

Figure 7-4. RSS Position Errors Range-Rate System with 104 Ground Stations

Table 7-3. RSS Position Errors for Various Initial Offsets Using Baseline Range Data Configuration With 104 Stations

Time from epoch (sec)	1 Mile Offset		5 Mile Offset		10 Mile Offset	
	RSS Error (ft)	RSS Standard Deviation (ft)	RSS Error (ft)	RSS Standard Deviation (ft)	RSS Error (ft)	RSS Standard Deviation (ft)
0	6000	10119	85563	15308	255,983	9,277
370	4031	2103	19010	2242		
1150	443	626	724	630		
1250	408	343	704	344		
1310	550	215	763	216		
1480	35	193	1103	196		
1550	116	186	949	188		
1780	14	81	306	81		
1800	17	83	319	83		
2300	208	92	318	92		
2490	216	81	249	81		
2700	277	80	191	80		

Table 7-4. RSS Position Errors for Various Initial Offsets Using Range Rate - Earth Disk System With 104 Stations

Time from Epoch (sec)	1 Mile Offset		5 Mile Offset		10 Mile Offset		20 Mile Offset	
	RSS Error (ft)	RSS Standard Deviation (ft)	RSS Error (ft)	RSS Standard Deviation (ft)	RSS Error (ft)	RSS Standard Deviation (ft)	RSS Error (ft)	RSS Standard Deviation (ft)
190	4365	10038	27071	11281	197,060	8730	786,183	5139
370	1928	1780	21395	1799	15914	1815	69107	1629
1150	251	624	6609	628	11815	625	84591	577
1250	90	343	1868	342	3397	340	26910	317
1310	201	215	2290	214	495	214	34591	215
1480	109	193	2290	191	6912	189	47852	194
1550	216	186	2961	184	6738	182	45376	183
1780	123	81	722	82	1882	82	14668	85
1800	131	83	762	83	1980	84	15453	87
2300	194	92	882	94	2688	95	22105	102
2490	132	81	806	81	2418	82	22312	84
2700	171	80	575	80	1825	81	17703	83

7.5 RANGE RATE WITH COMPLETE HORIZON SENSOR SYSTEM

From the above results, it appears that the full horizon sensor system of Section 5 should be investigated as a means of preventing convergence problems. The results of combining the baseline horizon sensor and range rate systems are summarized in Table 7-5. By comparing the results with those of Table 7-2, the utility of the horizon sensor as an effective means of bounding errors is quite evident. Furthermore, no significant degradation in behavior was noted when the system was faced with large initial errors.

Table 7-5. RSS Position Errors With Range Rate and Horizon Sensor Measurements

Time of Acquisition and Termination of Ground Station (sec)	Station Number	RSS Error (ft)	RSS Standard Deviation (ft)
0	--	11605	17321
930	19	11999	6963
990		2000	3240
1170	4	2010	3326
1320		782	2003
1560	3	2843	2394
1800		2320	1327
3180	10	12761	3398
3390		263	457
5400	--	1536	2359

8. ONE-WAY DOPPLER MEASUREMENTS TO KNOWN GROUND STATIONS

8.1 DISCUSSION

As shown in Sect. 7, range rate measurements to known landmarks appear to provide extremely accurate satellite navigation. Actually, range rate is a mathematical abstraction of a real process. If the results obtained thus far are to be meaningful, that process must be examined carefully.

Specifically, range rate data are actually data derived from doppler shifts of high frequency electromagnetic radiation. Practical systems, yielding what are commonly termed "one-way doppler measurements", consist of several ground stations located around the globe which continuously transmit a nominal carrier frequency (Refs. 45 and 52). When one of the ground stations becomes visible to a user satellite, the frequency of the signal received by the satellite is compared with the frequency of a stable onboard oscillator. The comparison ideally yields a difference frequency Δf that is directly proportional to the time-rate of change of the distance between the satellite and the ground station, $(\dot{\rho})$, that is,

$$\dot{\rho} = k\Delta f \tag{8-1}$$

However, since frequency is defined as the number of events per unit time, measurement of the desired frequency difference cannot be made instantaneously. Instead, each measurement must be taken over some finite interval $t_i \leq t \leq t_f$. In practice, the integral of the frequency difference over that interval is measured. Mathematically, the observation can be represented as

$$y = \int_{t_i}^{t_f} k\Delta f \, dt = \int_{t_i}^{t_f} \dot{\rho} \, dt = \rho(t_f) - \rho(t_i) \tag{8-2}$$

Although Eq. (8-2) can be divided by $t_f - t_i$ to yield the <u>average</u> range rate over that interval, it is more convenient to consider the range difference of Eq. (8-2) directly. In any case, it should be clear that instantaneous range rate is only an approximation to the actual data type.

In actual practice the satellite and ground frequency oscillators are not perfect. Over short intervals the error can be modeled with a range bias, a frequency offset and a frequency offset drift with white noise assumed on both the range bias and the frequency offset (Ref. 41). Thus, if the state vector is defined as

x_1, x_2, x_3 — ECI satellite position

x_4, x_5, x_6 — ECI satellite velocity

x_7 — instantaneous range bias, (ft)

x_8 — instantaneous frequency offset, (ft/sec)

x_9, x_{10}, x_{11} — ECI ground station position

x_{12}, x_{13}, x_{14} — ECI ground station velocity

x_{15} range to satellite at acquisition time (see Appendix E)

x_{16} rate of change of offset in frequency (ft/sec^2)

where

$$\begin{aligned} \dot{x}_7 &= x_8 + u \\ \dot{x}_8 &= x_{16} \\ \dot{x}_{16} &= 0 \end{aligned} \tag{8-3}$$

and u is white noise,

the measurement can be expressed as

$$y = \rho(t_f) + x_7(t_f) - \rho(t_i) - x_7(t_i) + v(t_f) - v(t_i) \tag{8-4}$$

where v is white noise. The error model of Eq. (8-3) may be represented as shown in Fig. 8-1.

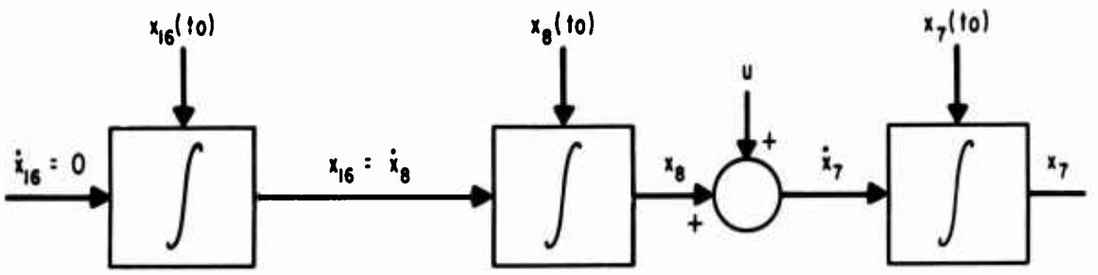

Figure 8-1. Block Diagram for One-Way Doppler Error Model

The measurements of Eq. (8-4) represent an additional problem when Kalman filtering processing is required. As formulated, the Kalman filter algorithm (Refs. 18, 19, 20, and 29) requires that the observations be expressed as a

function of the state vector at a specific time. The observation described in Eq. (8-4), however, involves the state at two different times, i.e., t_i and t_f. Thus an appropriate technique must be used to modify Eq. (8-4) so that compatibility with the Kalman filter can be obtained.

Three approaches were considered to resolve this difficulty. The first makes use of the range at acquisition as a state variable (Acquisition Range Reference Method), the second uses state extrapolation and is based on the difference between ranges at two successive observation times (Previous Range Reference Method), while the last method is based on range rate as an approximation to the actual measurement (Range Rate at Midpoint). A detailed development of these methods is provided in Appendix E.

8.2 BASELINE CONFIGURATION AND ASSOCIATED RESULTS

The baseline configuration used to examine one-way doppler systems is described in detail in Table 8-1.

8.2.1 The time history of the RSS position errors for the baseline case is shown graphically in Figure 8-2. A similar plot is given in Figure 8-3 for a case with the complete 104 ground stations of Appendix F.

8.2.2 The results obtained are very similar to the range-rate results of Sect. 7.

8.2.3 After 1-1/3 orbits with the baseline case, position errors are reduced to about 700 ft. After that, model errors become significant.

8.2.4 After 1/3 orbit, with the 104 station case, the position errors are reduced to about 300 ft. Thereafter, model errors become noticeable.

8.2.5 As shown in Appendix E, the use of the Acquisition Range Method involves a singular (i.e., at least one zero eigenvalue) covariance matrix at acquisition. At every sample time in the baseline simulation it was noted that one of the eigenvalues of the covariance matrix was close to zero in magnitude and not always positive. This situation, however, had no apparent effect on the performance of

Table 8-1. Baseline Configuration for One-Way Doppler Study

Key Parameters

Measurement Model	Acquisition Range Reference (see Appendix E)
Number of Stations	21
Gravity Model	Real World: APL "8-8" Filter World: μ and J_2
Atmosphere Model	Real World: U. S. Standard 1962 Filter World: exponential
Data Rate	1 sample/10 seconds
Measurement Noise	50 ft (1σ)
Forcing Noise	Real World: $\mathcal{E}[u(t)u(\tau)] = .01\ \delta(t-\tau)\ ft^2/sec^2$ (only on $\dot{x}_7$) Filter World: none

Initial Conditions

States	Real World	Filter World	Standard Deviation
x_1, x_2, x_3	Reference Orbit	6700 ft offset (estimated)	10,000 ft
x_4, x_5, x_6	Reference Orbit	6.7 ft offset (estimated)	10 ft/sec
x_7	10,000 ft	not estimated	---
x_8	5 ft/sec	0 ft/sec (estimated)	5 ft/sec
x_{15}	computed internally	computed internally	computed internally
x_{16}	.01 ft/sec^2	not estimated	---

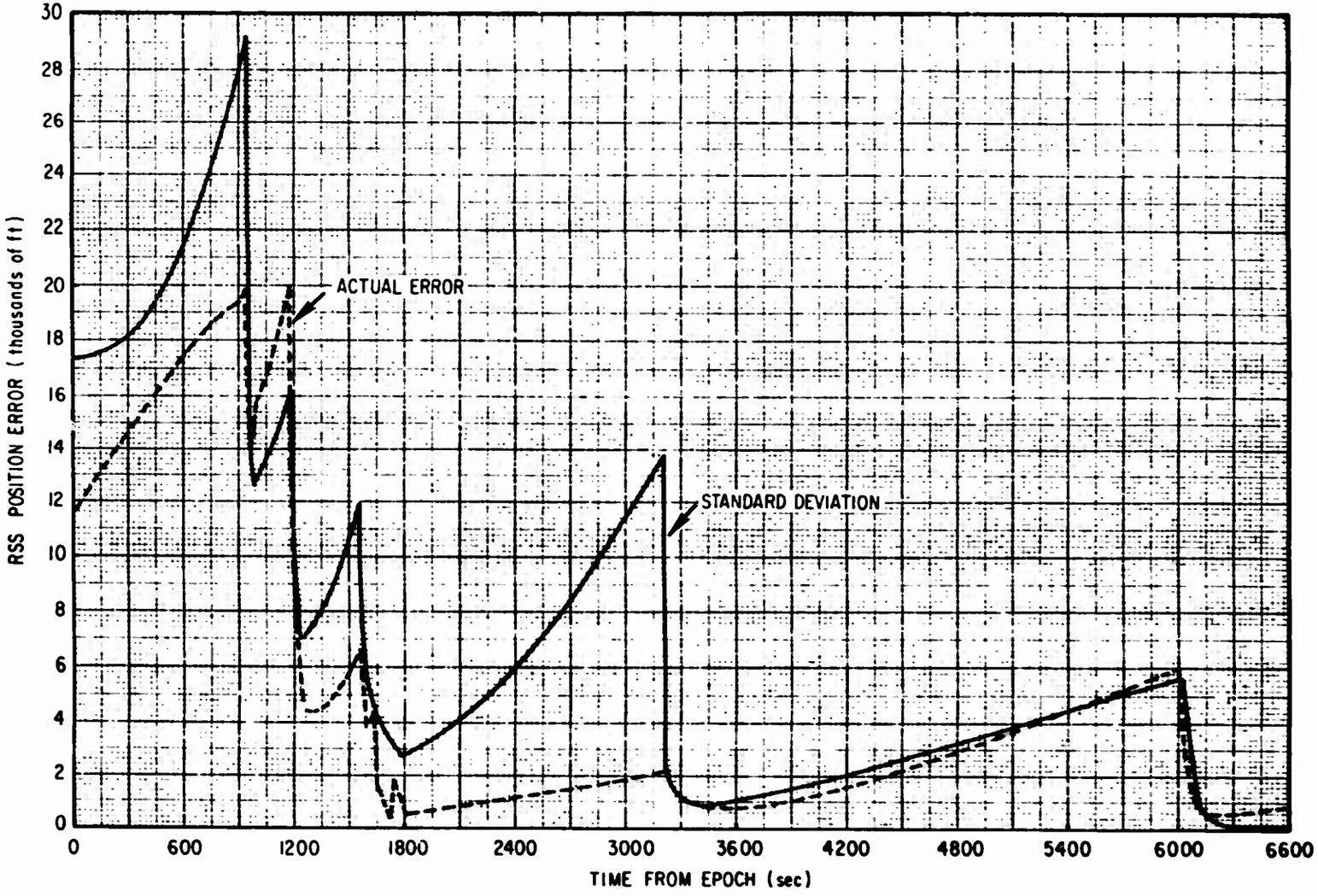

Figure 8-2. RSS Position Error for Baseline One-Way Doppler System

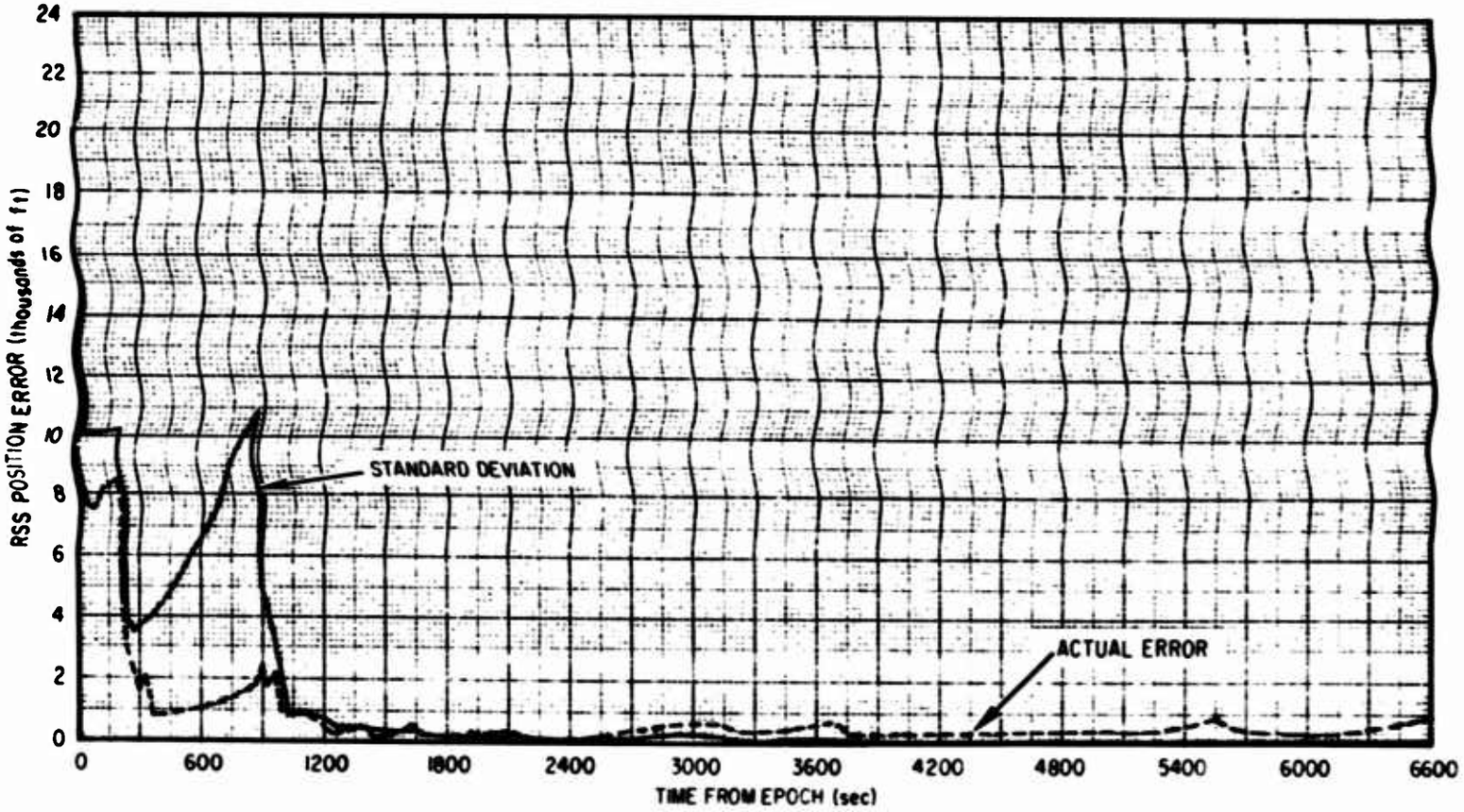

Figure 8-3. RSS Position Error for One-Way Doppler System with 104 Ground Stations

the filter on a computer with a 60-bit word. On the other hand, if a much smaller word length machine were used, roundoff could become a significant problem.

8.3 EFFECT OF DATA RATE

8.3.1 The baseline system with 104 ground stations was examined with data rates of 10, 20, and 30 sec. The full deployment of 104 ground stations was chosen to minimize the effect of stations whose visibility period is less than 30 sec. The results are summarized in Table 8-2.

Table 8-2. Effect of Data Rate on One-Way Doppler RSS Position Errors

Time from Epoch (sec)	10-sec Data Rate		20-sec Data Rate		30-sec Data Rate	
	RSS Error (ft)	Standard Deviation (ft)	RSS Error (ft)	Standard Deviation (ft)	RSS Error (ft)	Standard Deviation (ft)
0	11604	17321	11604	17321	11604	17321
1200	459	828	1108	1114	1056	1280
2400	145	153	479	218	264	261
3600	446	116	443	174	560	221
4200	237	54	165	76	266	95

8.3.2 For all rates examined, modeling error appears to become significant after about one-half an orbit. The effect is, of course, less prominent at the 30-sec data rate. In fact, with 21 ground stations and a 30-sec data rate, modeling error does not become significant until the second revolution.

8.3.3 Although the overall effect of increased data rates seems negligible as far as accuracy is concerned, a 10-sec rate is preferred over the slower rates since it may permit use of information from a station whose visibility is relatively short for a particular pass.

8.3.4 The 10-sec rate would also tend to accelerate convergence of the state for the frequency offset (x_8).

8.4 OSCILLATOR ERRORS

8.4.1 For the values considered, the effects of frequency offset drift, x_{16}, and the white noise forcing on $\dot{x}_7$ can be ignored by the filter.

8.4.2 In modeling the predicted range difference, the value of x_7 essentially cancels out; therefore, the quantity x_7 is unobservable. The presence of white noise on $\dot{x}_7$, of course, leads to a random walk on the measurement. However, since the duration of a pass is relatively short, the effect is not significant for the parameter values considered.

8.4.3 The unintentional frequency offset of the oscillators, x_8, is generally observable. For long-duration passes over a ground station, as shown in Table 8-3, almost all of this offset can be recovered by the end of the pass. While the offset rate may not be fully estimated for short passes, its net effect will, of course, be small in such cases.

Table 8-3. Observability of Frequency Offset for One-Way Doppler Measurement

Time from Station Acquisition (seconds)	Actual Frequency Offset (ft/sec)	Error in Estimated Frequency Offset (ft/sec)	Standard Deviation (ft/sec)
0	15	15	15
20	15	4.2	9.9
40	15	8.3	8.9
60	15	10.1	8.2
80	15	1.5	3.1
100	15	1.2	1.7
120	15	1.2	1.3
140	15	0.9	0.9
160	15	0.8	0.5
180	15	0.2	0.3
200	15	0.3	0.2
220	15	0.1	0.2

8.4.4 The frequency offset of the oscillators, x_8, must be estimated in the filter. This is obvious from Table 8-4 where the RSS position errors obtained when estimating or not estimating the drift are summarized.

Table 8-4. Effect of Frequency Offset Estimation on RSS Position Error

Time of Acquisition and Termination of Ground Station (sec)	Ground Station Number	5 ft/sec Offset		15 ft/sec Offset	
		Estimated (ft)	Not Estimated (ft)	Estimated (ft)	Not Estimated (ft)
0		11600	11600	11600	11600
940	19	19555	19555	19555	19555
980		3976	3696	4218	4117
1180	4	4588	4362	5046	4968
1310		551	6760	3307	20600
1560	3	1268	11282	4998	34256
1780		326	4650	887	11688
3200	10	1285	23177	5096	58779
3380		139	1297	917	3991

8.5 INITIAL CONVERGENCE ANALYSIS

As shown in Tables 8-5 and 8-6, the filter has difficulty converging for initial position offsets over three n mi. These results are similar to those obtained with range-rate data in Sect. 7 and suggest the need for horizon sensors.

Table 8-5. RSS Position Errors for Three n mi Initial Offset

Time from Epoch (sec)	104 Ground Stations		21 Ground Stations	
	RSS Error (ft)	Standard Deviation (ft)	RSS Error (ft)	Standard Deviation (ft)
0	31177	54772	31177	54772
1000	3078	403	19299	8589
1300	1265	170	32414	6807
1700	38	58	21622	846
3300	175	29	12501	535

Table 8-6. RSS Position Errors for Five n mi Initial Offset

Time from Epoch (sec)	104 Ground Station		21 Ground Stations	
	RSS Error (ft)	Standard Deviation (ft)	RSS Error (ft)	Standard Deviation (ft)
0	103923	173205	103923	173205
1000	763111	663	181828	13533
1300	147091	115	415801	1305
1700	83546	67	751210	212
3300	42811	28	3582780	45

8.6 STATION LOCATION ERRORS

The effect of errors in the location of the ground stations was investigated. In Tables 8-7 and 8-8 the results of estimating these errors or ignoring them completely are summarized. It is concluded that they should be estimated if their expected value is more than 100 ft.

Table 8-7. Effect of Station Location Errors at 2400 Sec on RSS Position Errors

Station Location Errors (ft)	Estimated		Not Estimated	
	RSS Error (ft)	RSS Standard Deviation (ft)	RSS Error (ft)	RSS Standard Deviation (ft)
0	264	261	264	261
50	251	271	269	261
200	354	543	456	261
400	693	698	831	261

Table 8-8. Effect of Station Location Errors at 4200 Sec on RSS Position Errors

Station Location Errors (ft)	Estimated		Not Estimated	
	RSS Error (ft)	RSS Standard Deviation (ft)	RSS Error (ft)	RSS Standard Deviation (ft)
0	265	95	265	95
50	323	106	344	95
200	396	286	583	95
400	601	412	903	95

8.7 MEASUREMENT MODELING APPROACH EVALUATION (SEE APPENDIX E)

8.7.1 Three methods for modeling the data were discussed in Section 8.1. A comparison of the Acquisition Reference Range (ARR) and the Previous Reference Range (PRR) methods for baseline conditions is summarized in Table 8-9. The ARR method gives somewhat better navigation accuracies. This result can be misleading since it is quite dependent on the validity of the real-world data model used. In this model, it was implicitly assumed that measurement noise occurs

only upon readout of the accumulated range difference. From this, it follows that the assumption of white noise in filter is strictly correct only for the ARR method. Furthermore, in the ARR method, the effect of this readout noise is clearly diminished with each successive measurement. Thus, considering that the assumed real-world model is quite unfavorable to the PRR method, that approach appears to give remarkably good results.

8.7.2 Indeed, even if the real-world model were correct, there are several distinct advantages with the PRR method. The dimension of the state vector is smaller, covariance initialization is not required, and, if the noise on $\dot{x}_7$ is truly significant, the resulting random walk effect would considerably degrade the ARR method but not the PRR method.

Table 8-9. Comparison of RSS Position Errors Obtained by Acquisition Acquisition Range Reference and Previous Range Reference Methods

Time from Epoch (sec)	Acquisition Reference Range Method		Previous Reference Range Method	
	RSS Error (ft)	Standard Deviation (ft)	RSS Error (ft)	Standard Deviation (ft)
0	11605	17321	11605	17321
1200	1056	1280	764	1490
2400	264	261	254	242
4200	266	95	422	148

8.7.3 The use of instantaneous range rate computed at the middle of a data collection interval as an approximateion to the measured average range rate over that interval was tested by a series of simulations in which the collection interval was varied from 1 to 10 sec. For all cases, a new measurement was taken every 10 sec. The results, which are summarized in Table 8-10, show that the approximation is only valid for collection intervals less than 5 sec.

8.7.4 In a separate study, the average range rate and the instantaneous value at the midpoint of the 10 second data intervals were directly compared for various orbital and ground station configurations. The study showed that the approximation in question is quite good near the time of satellite rise or set, but is generally quite poor (up to 1 n mi/sec error) at the time of closest approach. Upon careful examination, this effect was observed in the simulation runs which tested this approximation. That is, the filter seemed to perform adequately near each station acquisition, but eventually became "confused". Eventually, of course, this confusion lead to filter divergence.

Table 8-10. RSS Position Errors Obtained by Use of Instantaneous Range Rate for Processing One-Way Doppler Data

Time from Epoch (sec)	Accumulation Period for Range-Rate Approximation (New Accumulation every 10 sec for all cases)					
	10 seconds		5 seconds		1 second	
	RSS Error (ft)	Standard Deviation (ft)	RSS Error (ft)	Standard Deviation (ft)	RSS Error (ft)	Standard Deviation (ft)
0	11605	17321	11605	17321	11605	17321
1000	14600	12894	15206	12909	15331	12878
1300	2726	6520	742	6479	315	6546
1800	31363	17349	7694	1521	317	1642
3400	2656	715	683	678	44	697

9. TWO ANGLES TO KNOWN LANDMARKS

9.1 BASELINE CONFIGURATION AND RESULTS

Although extremely high accuracy navigation was shown to be possible with range rate (or one-way doppler) systems; there is an admitted loss of autonomy. It is possible that such accuracy would be obtained with somewhat more autonomy by means of angular measurements to known locations. Such measurements could be obtained in practice by either optical tracking of known surface features or antenna tracking of electromagnetically radiating cooperative or uncooperative sources. In this section the generic problem of navigating with such measurements is considered. The specific baseline configuration used for this study is described in Table 9-1.

The results of simulating the baseline case are shown graphically in Fig. 9-1 and summarized in Table 9-2. As might be anticipated, the general behavior of angular measurements is quite similar to range rate measurements. Indeed, the results seem somewhat more stable during the first orbit.

9.2 EFFECT OF INCREASED SENSOR ACCURACY

As indicated by comparison of Tables 9-2 and 9-3 improving the sensor accuracy to 30 arc sec has little effect during the first three landmarks while performance is enhanced by a factor of two after the third landmark.

9.3 EFFECT OF HORIZON SENSOR AUGMENTATION

The results obtained by adding the basic horizon sensor configuration of Sec. 5 to the 30-arc sec dual-angle measurement system are shown in Fig. 9-2 and summarized in Table 9-4. The horizon sensor system effects a marked improvement in performance with the first two landmarks, but does not significantly change the steady-state errors.

9.4 EFFECT OF INCREASING LANDMARKS

The 30-arc sec dual-angle system augmented with horizon sensors was studied with the full landmark deployment of Appendix F. The improved performance of the system is clearly seen in Table 9-5.

Table 9-1. Baseline Configuration for Two Angles to Known Landmarks

Key Parameters

Measurement Model	Right ascension and declination to landmark using an inertial coordinate system centered at the navigator
Number of Stations	21
Gravity Model	Real world: APL "8-8" Filter world: μ and J_2
Atmosphere Model	Real world: U.S. Standard 1962 Filter world: Exponential
Data Rate	1 sample/10 seconds
Measurement Noise	60 arc sec on each angle
Forcing Noise	None
Minimum elevation angle for landmark visibility	5 deg

Initial Conditions

State	Real World	Filter World (all states estimated)	Standard Deviation
x_1 x_2 x_3 (position)	Reference Orbit	6700 in each direction	10,000 ft
x_4 x_5 x_6 (velocity)	Reference Orbit	6.7 ft/sec in each direction	10 ft/sec

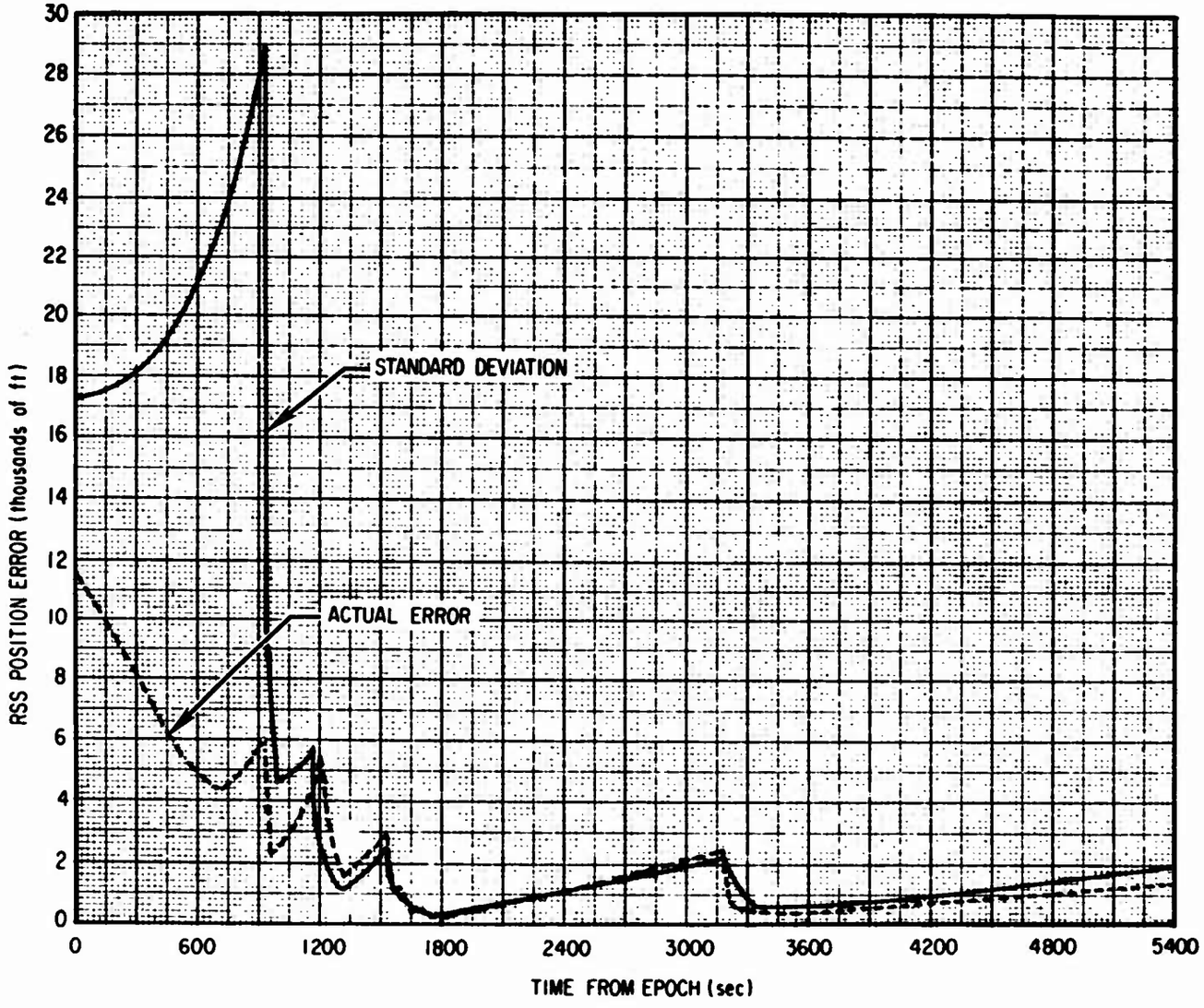

Figure 9-1. RSS Position Errors for Baseline Dual-Angle System

Table 9-2. RSS Error for Dual-Angle Baseline System

Time of Acquisition and Termination of Landmark (sec)	Landmark Number	RSS Error (ft)	RSS Standard Deviation (ft)
0	--	11604	17320
930	10	6045	28938
990		2416	4663
1170	4	4490	5669
1320		1618	1131
1530	3	2901	2453
1800		309	286
3180	10	2486	2247
3390		293	637
5400	--	1394	2046

Table 9-3. RSS Errors for Dual-Angle System Using 30 Arc Sec Angle Errors

Time of Acquisition and Termination of Landmark (sec)	Landmark Number	RSS Error (ft)	RSS Standard Deviation (ft)
0	--	11604	17320
930	19	6044	28938
990		914	2778
1170	4	3230	4278
1320		661	623
1560	3	877	1746
1800		112	144
3180	10	877	1139
3390		233	319
5400	--	1332	1028

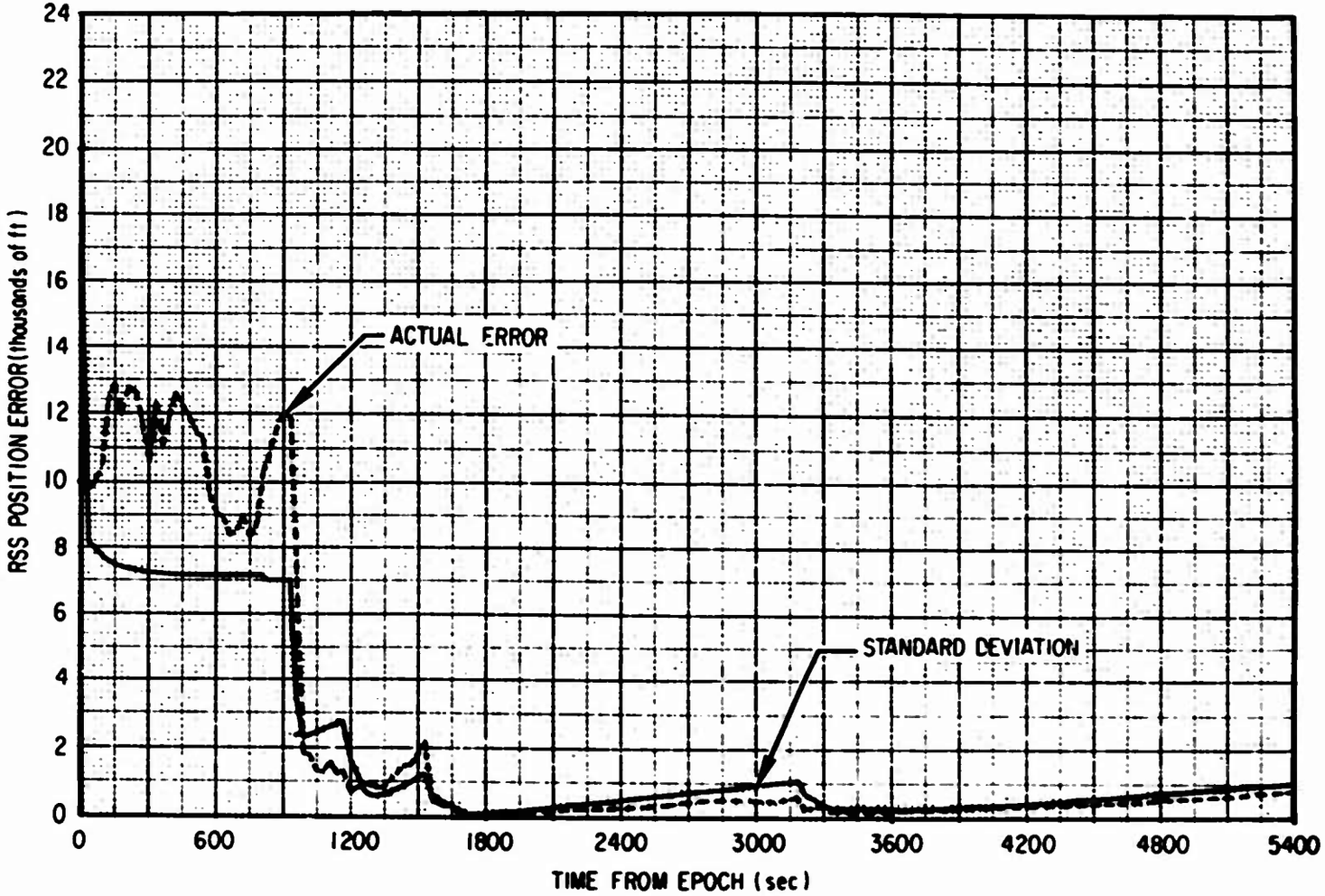

Figure 9-2. RSS Position Errors for Dual-Angle Horizon Sensor Configuration (Using 30 arcsec Angle Errors)

Table 9-4. RSS Position Errors for Dual Angle-Horizon Sensor System Using 30 Arc Sec Angular Errors

Time of Landmark Acquisition and Termination (sec)	Landmark Number	RSS Position Error (ft)	RSS Standard Deviation (ft)
0	--	11604	17320
930	19	11973	6963
990		1786	2342
1170	4	1288	2787
1320		797	563
1530	3	2078	1193
1800		88.4	142
3180	10	622	1093
3390		196	318
5400	--	805	1004

9.5 EFFECT OF MULTIPLE SIMULTANEOUS LANDMARK TRACKING ON CONVERGENCE

From previous results, it is clear that the use of horizon sensors is a good approach for ensuring convergence from large initial position errors. As a possible alternative, the use of simultaneous tracking of more than one landmark is of interest. To examine this approach, a configuration with three different sets of 30-arc sec angle trackers was devised and simulations were performed for initial errors of 1, 5, 10, and 20 n mi. Perfectly matched dynamic models were used in order to isolate the cause of possible divergence.

The results, as summarized in Table 9-6, show that convergence is not possible for large initial errors if only a filter algorithm is used. However, some special initialization procedure such as triangulation using simultaneous measurements to two landmarks could possibly be used effectively.

Table 9-5. RSS Position Errors for Dual-Angle 30 Arc Second Error-Horizon Sensor System with 104 Landmarks

Time of Acquisition and Termination of Landmarks (sec)	Landmark Number	RSS Error (ft)	RSS Standard Deviation (ft)
0 190	80	11604 3534	17320 1789
200 390	72	649 433	469 448
870 1150	63	1295 45.3	1111 96.7
1160 1250	26	39.6 31.3	97.3 102
1260 1310	4	30.9 47.9	104 104
1320 1480	23	48.4 52.2	106 73.1
1490 1560	25	48 74.7	73.7 78.4
1560 1780	3	74.7 85.1	78.4 67.4
1790 1830	24	89.1 102	67.9 70.9
2070 2310	68	156 109	94.1 77.5
2310 2520	70	110 116	77 75
2550 2820	40	121 135	77.9 76.3
3000 3300	88	169 130	89 78.6
3310 3390	10	129 132	78.8 81
3540 3930	93	135 150	91.9 76.6
3940 4020	56	162 161	76.8 79.8
4020 4290	57	166 97.3	79.1 71.6
5400	--	203	138

Table 9-6. RSS Position Errors for Three Simultaneous Dual-Angle Trackers

Time From Epoch (sec)	1 Mile Offset		5 Mile Offset		10 Mile Offset		20 Mile Offset	
	RSS Error (ft)	RSS Standard Deviation (ft)	RSS Error (ft)	RSS Standard Deviation (ft)	RSS Error (ft)	RSS Standard Deviation (ft)	RSS Error (ft)	RSS Standard Deviation (ft)
0	11604	17320	58023	86602	116047	173205	232095	246410
370	655	705	1438	717	3425	722	10510	731
870	1058	1472	1020	1486	2849	1491	10466	1503
1810	24.9	106	61.8	106	191	106	666	107
2090	63.5	150	98	150	292	150	1049	151
2500	42.8	138	97	138	250	139	780	139
2550	40	144	96.5	145	252	145	795	145
2700	36.2	140.6	82.2	140	228	140	750	141

10. OTHER SYSTEMS

Since the time available for the current study was quite limited, only those systems which a priori appeared to provide an optimum combination of accuracy, autonomy, and cost could be studied in detail. In this section some of the systems which were not simulated are discussed qualitatively.

10.1 NAVIGATION SATELLITES

For several years, the concept of navigation by observing specially designed satellites has received considerable attention (Ref. 44). The following key arguments are noted:

10.1.1 Since navigation satellites would essentially be known points in inertial space, the accuracy performance should be at least comparable to range or range-rate observations to ground stations. Performance with angle measurements would depend strongly on the relative distance between the user and the navigation satellite.

10.1.2 A very attractive property of satellites is their wide range of visibility as compared to ground stations. In particular, with synchronous navigation satellites, the coverage area is practically a hemisphere for low-altitude navigators. Indeed, the coverage area grows even larger as the navigator's altitude increases. Global coverage could easily be obtained with a relatively small number of satellites if they were properly located.

10.1.3 In order to use satellites for navigational observations, their ephemerides must be maintained. This implies the utilization of a ground-based tracking network and complex. Clearly, such a system cannot inherently provide a high degree of autonomy to a user.

10.2 EJECTED PROBE

The concept of orbit navigation by observing a secondary "mini" satellite which has been ejected from the primary vehicle has recently been investigated (Ref. 38). The relative motions of the two satellites when coupled with the dynamical models for both can theoretically provide enough information for navigation in inertial space. However, the accuracies reported in the reference are not very encouraging. Even if all model errors were neglected, accuracies of only 3633, 1739, and 1358 feet after 1, 2, and 3 orbits, respectively, were indicated. Nevertheless, because of the inherent high degree of autonomy, the concept should be analyzed further before it is completely eliminated from consideration.

10.3 STAR-HORIZON MEASUREMENTS

A possible approach to autonomous navigation could be based on observing the angle between a known star and the horizon of the earth as measured in the plane defined by the navigator, the star, and the center of the earth. The information contained in this so-called "star-horizon" or "star-elevation" measurement is essentially the same as that of the horizon sensor measurement described in Section 5; that is, since horizon sensor measurements inherently require precise attitude information and since such data can only be achieved by using star observations, the horizon sensors effectively measure angles between the stars and the horizon. The basic difference lies in the mechanization. While stars must be acquired by the star-elevation sensor, there is no need for high precision attitude information. Another important distinction between the two types of measurements resides in the fact that horizon sensor observations are always made in the planes of the sensor heads, while the star-horizon measurement plane varies with the stars being used.

It was shown in Section 5 that deterministic navigation was theoretically possible using horizon sensors. It can be shown that three properly oriented star-elevation measurements could also provide such a capability. Thus no significant difference in performance should be expected between these two measurement types.

10.4 STAR OCCULATION

Another approach to autonomous navigation involves measurement of the time at which selected stars pass behind the earth's horizon. While this star occulation is physically quite different from the star-elevation observation described in Section 10.3, the navigation information contained in both measurements is basically the same. It can be shown (Ref. 3) that both measurements provide position information normal to the line of sight to the horizon in a plane defined by the navigator, the star, and the center of the earth.

The major difference between these two sensors lies in the phenomena measured; that is, horizon sensors depend on the carbon dioxide absorption layer of the atmosphere, while the occulation measurement would depend on the instantaneous atmospheric refraction and absorption of light at the time of measurement. Notwithstanding these model differences, however, the convergence properties of an occulation system should be similar to the horizon sensing system already discussed. Specification of the accuracy attainable would, of course, depend on detailed model analysis and simulation.

11. COMPUTER WORDLENGTH EFFECTS

Numerical roundoff difficulties in recursive filtering have been widely studied and publicized in recent years. Although many techniques for alleviating these difficulties have been suggested, all are ultimately limited by the basic wordlength of the machine used to process data.

In order to determine the sensitivity of satellite navigation to such computer characteristics, two baseline configurations with supposedly different numerical properties were simulated with a variety of wordlengths. Square root filtering was used in all cases to enhance the overall performance. The unknown landmark horizon sensor baseline configuration was used as one standard because of the relatively high dimensional state vector (14) involved, and also because unknown landmark tracking has been reported to be particularly sensitive to numerical errors. To maintain perspective, the straightforward case of range rate to known landmark was chosen as the other basic example. This configuration required only six states for navigation and no peculiar numerical problems were noted.

All simulations were performed on a Control Data 6600 60-bit wordlength machine by means of special software which could truncate the results of selected arithmetic operations. To compensate for optimum coding that would undoubtedly be provided for operational navigation software, only those calculations directly associated with matrix multiplication, addition, or subtraction were actually subjected to truncation. That is, matrix inversion, square-root extraction, integration, and partial derivative computations were all performed with the full 60 bit word of the 6600 computer. The results reported should be highly optimistic, since failure of a simulated truncation under these conditions would surely imply failure if all operations were truncated.

Under the above assumptions, the baseline configurations chosen were simulated with 60, 30, 20 and 15 bit words. The results obtained are summarized in

Tables 11-1 and 11-2. Comparison of these tables shows that in spite of the advertised numerical differences, the configurations behaved remarkably similar with respect to wordlength limitation. It appears that a 30-bit machine would be adequate for both systems, while use of only 20 bits could result in considerable numerical difficulty. Since the study was admittedly highly optimistic, it is not likely that machines with less than 20 bits could be effective for navigation.

The authors would like to acknowledge the assistance of Dr. H. J. Wertz, who prepared the special software that was used to simulate the various computer wordlengths.

Table 11-1. Effect of Computer Wordlength With Baseline Unknown Landmark Tracking - Horizon Sensor Configuration

Time from Epoch (sec)	60 BITS		30 BITS		20 BITS		15 BITS
	RSS Error (ft)	RSS Standard Deviation (ft)	RSS Error (ft)	RSS Standard Deviation (ft)	RSS Error (ft)	RSS Standard Deviation (ft)	
0	11604	17320	11604	17320	11574	17320	Failed immediately
1020	1356	2532	2348	2532	16199	2306	
2010	1668	1381	1657	1381	6798	1328	
3000	540	2599	540	2599	10497	2473	
4000	598	611	587	611	12383	602	

Table 11-2. Effect of Computer Word Length With Baseline Range Rate to Known Landmarks Configuration

Time from Epoch (sec)	60 BITS		30 BITS		20 BITS		15 BITS	
	RSS Error (ft)	RSS Standard Deviation (ft)	RSS Error (ft)	RSS Standard Deviation (ft)	RSS Error (ft)	RSS Standard Deviation (ft)	RSS Error (ft)	RSS Standard Deviation (ft)
0	11604	17320	11604	17320	11574	17320	10407	17320
1000	573	619	573	619	1244	619	26035	599
2090	121	118	122	118	2051	118	69823	116
3010	441	104	445	104	4994	104	155941	103
4000	341	68	347	68	6558	68	215481	64

12. PRIMARY CONCLUSIONS

12.1 Horizon sensors appear to be a promising candidate for inclusion in hybrid autonomous navigation systems in order to provide recovery from large off-nominal conditions, bound maximum errors, and accelerate filter convergence. On the other hand, the use of horizon sensors alone can only provide coarse navigation accuracy.

12.2 The convergence properties of horizon sensor systems are enhanced by inclusion of the measurement of the angle subtended by the earth's disk.

12.3 The ability to recover from large initial errors is not a natural characteristic of many navigation configurations. The associated problem generally requires special attention.

12.4 Unknown landmark tracking, while attractive from an autonomy point of view, provides only moderate accuracy with oscillatory behavior unless a high accuracy sensor and a relatively uniform distribution of landmarks with small altitude uncertainties are ensured. To achieve this uniform distribution of landmarks, the night-day and cloud-cover problems must be solved.

12.5 Systems utilizing optical or electronic measurements (e.g., range, Doppler, or angular measurements) to known landmarks or satellites can be used to provide high navigation accuracy. The position accuracy of the landmarks or satellites is generally more critical than the choice of the sensor type used.

12.6 Even in the presence of time-varying oscillator model errors, one-way Doppler systems can yield excellent navigation accuracy. Because of the short duration of a station pass, the only oscillator error that need be modeled in the filter is a constant frequency offset error between the ground and user oscillators. This error is generally observable for those stations close to the orbit plane.

12.7 Computers for satellite navigation with 30-bit word lengths appear to be adequate for avoiding filter divergence due to numerical round-off. Based on the highly optimistic study performed, it is not likely that machines with less than 20 bit words could be effective for navigation.

APPENDIX A

REAL WORLD DYNAMIC MODELS

A.1 GEOPOTENTIAL

In general, geopotential forces can be found by computing gradients of truncated versions of the function

$$U = \frac{\mu}{r}\left\{1 + \sum_{n=2}^{\infty}\left(\frac{Re}{r}\right)^n\left[C_n P_n(\sin\phi) + \sum_{m=1}^{n} P_n^m(\sin\phi)(C_{nm}\cos m\lambda + S_{nm}\sin m\lambda)\right]\right\}$$

where

μ is the product of the universal gravitational constant and the mass of the earth

r, ϕ, and λ are the vehicle distance from the center of the earth, the vehicle geocentric latitude, and the vehicle longitude

Re is the earth's equatorial radius

P_n are the Legendre polynomials of the first kind of degree n

P_n^m are associated Legendre functions of the first kind of degree n and order m

C_n are zonal harmonics

C_{nm}, S_{nm} are nonzonal (sectoral and tesseral) harmonics

The specific truncation and appropriate coefficients for the model used in SNAP were adopted from John Hopkins Applied Physics Laboratories (APL) "8-8" model (Refs. 17 and 30). The values used are given in Table A-1 and are based on the following normalization formulas.

$$\overline{C}_{nm} = KC_{nm}$$

$$\overline{S}_{nm} = KS_{nm}$$

$$K = \left[\frac{(n + m)!}{(n - m)!}\right]^{1/2}$$

A.2 ATMOSPHERE

The atmosphere model used was the United States Standard Atmosphere, 1962 (Ref. 43). A ballistic coefficient of 0.02 ft^2/lb was used.

Table A-1. Values for $\overline{C}_{mn}$ and $\overline{S}_{mn}$ for APL "8-8" Geopotential Model

n		0	1	2	3	4	5	6	7	8
2	$\overline{C}$	-1082.7	0	7.53						
	$\overline{S}$	0	0	-3.79						
3	$\overline{C}$	2.676	6.90	4.56	2.47					
	$\overline{S}$	0	0.80	-2.54	3.66					
4	$\overline{C}$	1.4	-2.39	1.77	3.59	-0.89				
	$\overline{S}$	0	-187	1.88	0.03	0.81				
5	$\overline{C}$	0.028	0.64	1.26	0.43	-2.29	-0.16			
	$\overline{S}$	0	-0.78	-1.58	0.49	-1.22	-3.14			
6	$\overline{C}$	-0.37	0	-0.82	2.70	-1.56	-0.90	0.07		
	$\overline{S}$	0	0.51	-0.79	0.26	-2.59	-2.60	-1.18		
7	$\overline{C}$	0.593	0.69	2.51	2.16	-0.75	-0.31	-2.49	0.48	
	$\overline{S}$	0	0.51	0.33	-1.13	0	-1.02	4.15	-0.79	
8	$\overline{C}$	-0.07	-0.86	0.55	0.32	-0.40	0.47	-0.13	0.99	-0.85
	$\overline{S}$	0	-0.28	-0.22	1.26	0.22	-0.01	3.88	-0.41	0.55
9	$\overline{C}$	-0.177								
	$\overline{S}$	0								
10	$\overline{C}$	0.5								
	$\overline{S}$	0								
12	$\overline{C}$	-0.31								
	$\overline{S}$	0								

Note: All coefficients are in units of 10^{-6} (APL normalization)

APPENDIX B

FILTER WORLD DYNAMIC MODELS

B.1 GEOPOTENTIAL

Filter computations were based on the simple geopotential function

$$U = \left[\mu/r - \left(\mu R_e^2/r^3\right)\right] J_2 P_2(\sin \phi)$$

where the notation is identical to that of Appendix A and $J_2 \equiv - C_2$.

B.2 ATMOSPHERE

The densities used were computed from a formula developed by Schusterman (Ref. 40); that is, the density ρ at an altitude z above the earth was found according to

$$\rho = \rho_0 \left[\frac{a}{a + b(z - z_0)}\right]^{1/b} \frac{gm}{cm^3}$$

where

$a = 16.4$ km
$b = 0.232$
$\rho_0 = 3.951 \times 10^{-12}$ gm/cm^3
$z_0 = 140$ km

A ballistic coefficient of 0.02 ft^2/lb was used.

APPENDIX C

REFERENCE ORBIT

Four representations for the initial conditions of the reference orbit are given below. Key fundamental constants are:

Epoch date = 2230 GMT, 29 Feb. 1980

$\mu = 1.4076538841 \times 10^{16}$ ft^3/sec^2

Earth radius = 20,925,738 ft

Earth rotation rate = 4.1780742×10^{-3} deg/sec

1. Earth-Centered Inertial (ECI). Based on an earth-centered coordinate system with an equatorial x-y plane whose x and z axes are directed to the mean equinox and north pole, respectively.

   $x = -1.59387494563 \times 10^{7}$ ft

   $y = 1.51831714534 \times 10^{7}$ ft

   $z = 3.84199431557 \times 10^{-15}$ ft

   $\dot{x} = 6.16441282935 \times 10^{3}$ ft/sec

   $\dot{y} = 6.00674668844 \times 10^{3}$ ft/sec

   $\dot{z} = 2.36312409387 \times 10^{4}$ ft/sec

2. Spherical

   Right ascension (positive east from x-axis) = 136.390753744 deg

   Geocentric declination = 1.0×10^{-20} deg

   Angle between velocity vector and geocentric vertical = 90.7298014230 deg

   Azimuth of velocity vector from north (A_z) = 340 deg

   Magnitude of position vector (R) = $2.20130059195 \times 10^{-7}$ ft

   Magnitude of velocity vector (V) = $2.51498815029 \times 10^{4}$ ft/sec

3. Classical

Semi-major axis = $2.17763946916 \times 10^{7}$ ft

Eccentricity = $1.67413647743 \times 10^{-2}$

Inclination = 110 deg

Right ascension of ascending node = 136.390753744 deg

Argument of perigee = 131.193639651 deg

Time of last perigee passage = -3442.155976 sec from epoch

4. Geographic

Geodetic latitude = 0 deg

Geodetic longitude = 360 deg

Angle between velocity vector and geocentric horizontal = -0.7298014230 deg

Az = 340 deg

R = $2.2013005915 \times 10^{7}$ ft

V = $2.51498815029 \times 10^{4}$ ft/sec

APPENDIX D

HORIZON ERROR MODEL

As described in Sect. 5.1, the measurements considered to be made by horizon sensors are the direction of the local vertical defined by θ_1 and θ_1' and the angle subtended by the widest diameter of the earth's apparent disk θ_2. Actually, θ_1', θ_1, and θ_2 cannot be measured directly but are inferred from the directions to the horizons. The plane defined by the z_3-axis (see Figures 5-1, 5-2, and the apparent center of the earth is shown in Figure D-1. The angles α_{1n} and α_{2n} are the expected measurements to the nominal CO_2 absorption layer, while the angles α_1 and α_2 are the instantaneous measurements to the true CO_2 absorption layer. The measurements can be thus expressed as

$$\begin{aligned} \alpha_1 &= \alpha_{1n} - \delta\alpha_1 + u_1 \\ \alpha_2 &= \alpha_{2n} + \delta\alpha_2 + u_2 \end{aligned} \qquad \text{(D-1)}$$

where $\delta\alpha_1$ and $\delta\alpha_2$ are the errors due to the uncertainty in the altitude of CO_2 absorption layer at the point of tangency, while u_1 and u_2 are white noise processes representing sensor noise.

The horizon errors have been statistically described by autocorrelation functions. Simulation of this type of error is readily achieved by means of first-order Markov processes. Before this can be done, however, the complete autocovariance matrix must be known. Mc Arthur (Ref. 34) indicates that the errors in the altitude of the CO_2 absorption layer are exponentially correlated in space and time with a great circle space constant of 2500 n mi and a time constant of 10 days. The variance is reported to be 2887^2 ft^2.

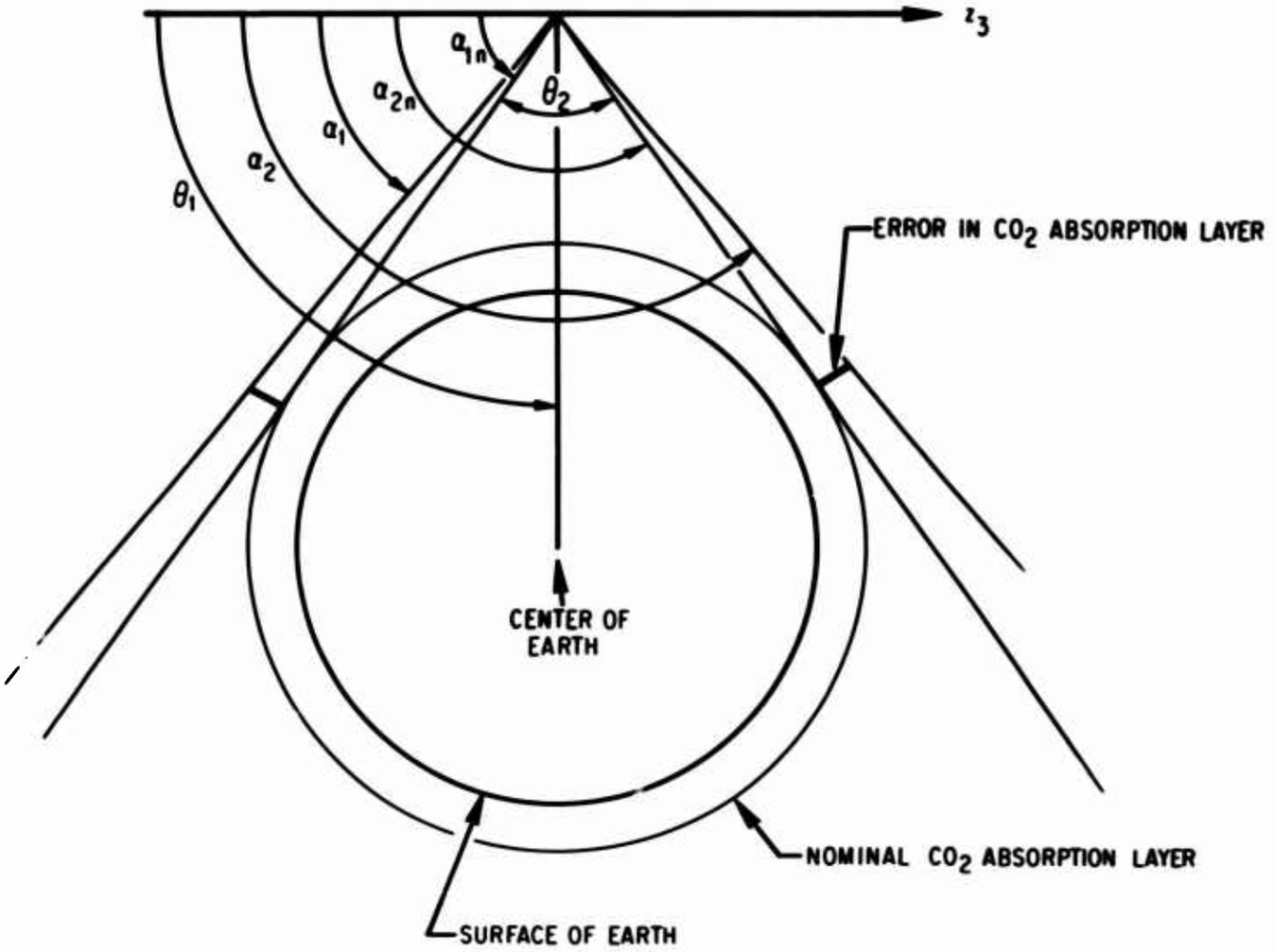

Figure D-1. Horizon Error Geometry

If an altitude of 100 n mi is considered, the impact of this error on the measurement can be computed by using the distance to the horizon (916.2 n mi) to compute the equivalent angular uncertainty

$$\sigma_1 = \left(\frac{2887 \text{ ft}}{916.2 \text{ n mi}}\right)\left(\frac{1 \text{ n mi}}{6076 \text{ ft}}\right)\left(\frac{57.3 \text{ deg}}{1 \text{ rad}}\right) = 0.02971 \text{ deg} \qquad \text{(D-2)}$$

Further, since the vehicle's ground trace travels along the surface of the earth at an average rate of 4 n mi/sec, an equivalent time constant of the space correlation can be computed as:

$$t_c = 2500 \text{ n mi } (1 \text{ sec}/4 \text{ n mi}) = 625 \text{ sec} \qquad \text{(D-3)}$$

An approximation for the autocovariances of $\delta\alpha_1$ and $\delta\alpha_2$ can now be written as

$$\begin{aligned} [\delta\alpha_1(t)\delta\alpha_1(t+\tau)] &= \sigma_1^2 \exp[-(t-\tau)/t_c] \\ [\delta\alpha_2(t)\delta\alpha_2(t+\tau)] &= \sigma_2^2 \exp[-(t-\tau)/t_c] \end{aligned} \qquad \text{(D-4)}$$

where $\sigma_1^2 = \sigma_2^2 = 0.02971^2 \text{ deg}^2$ and $t_c = 625$ sec. Note that the 10 day time constant has been neglected for this approximation since it is much longer than the period of an orbit, which was the duration of a typical simulated flight.

To determine the cross correlation between $\delta\alpha_1$ and $\delta\alpha_2$, one can consider the great circle separation distance between the points of tangency of the two lines to the horizons. For the orbit considered in this study, the separation distance, ΔD, varies from 1423 to 2547 n mi. Evaluating the appropriate exponentials results in an average correlation coefficient of approximately

$$\rho = \exp(-\Delta D/2500) \approx 0.5 \qquad \text{(D-5)}$$

Thus

$$\mathcal{E}[\delta\alpha_1(t)\delta\alpha_2(t+\tau)] = \rho\sigma_1\sigma_2 \exp[-(t-\tau)/t_c]$$
$$= (0.5)(0.0297)^2 \exp[-(t-\tau)/t_c] \qquad \text{(D-6)}$$

At this point, enough information about $\delta\alpha_1$ and $\delta\alpha_2$ is known to simulate their influences on the measurements by means of Markov processes. From Figure D-1, it can readily be shown that θ_1 and θ_2 are linearily related to α_1 and α_2 by the transformation

$$\begin{bmatrix}\theta_1\\ \theta_2\end{bmatrix} = A\begin{bmatrix}\alpha_1\\ \alpha_2\end{bmatrix} \qquad \text{(D-7)}$$

where

$$A = \begin{bmatrix}\frac{1}{2} & \frac{1}{2}\\ -1 & 1\end{bmatrix}$$

From Eq. (D-1) and (D-7) the autocovariance of the horizon errors in θ-space can be found to be

$$\mathcal{E}[\delta\theta(t)\delta\theta^T(t+\tau)] = A\mathcal{E}[\delta\alpha(t)\delta\alpha^T(t+\tau)]A^T \qquad \text{(D-8)}$$

where

$$\delta\theta = A\delta\alpha$$

$$\delta\alpha = \begin{bmatrix} -\delta\alpha_1 \\ \delta\alpha_2 \end{bmatrix}$$

$$\delta\theta = \begin{bmatrix} \delta\theta_1 \\ \delta\theta_2 \end{bmatrix}$$

Expanding Eq. (D-8),

$$\mathcal{E}[\delta\theta(t)\delta\theta^T(t+\tau)]$$

$$= \begin{bmatrix} \frac{1}{2} & \frac{1}{2} \\ -1 & 1 \end{bmatrix} \mathcal{E} \begin{bmatrix} \delta\alpha_1(t)\delta\alpha_1(t+\tau) & -\delta\alpha_1(t)\delta\alpha_2(t+\tau) \\ -\delta\alpha_2(t)\delta\alpha_1(t+\tau) & \delta\alpha_2(t)\delta\alpha_2(t+\tau) \end{bmatrix} \begin{bmatrix} \frac{1}{2} & \frac{1}{2} \\ -1 & 1 \end{bmatrix}^T$$

$$= \exp\left[-\frac{(t-\tau)}{t_c}\right] \begin{bmatrix} \frac{1}{2} & \frac{1}{2} \\ -1 & 1 \end{bmatrix} \begin{bmatrix} \sigma_1^2 & -\sigma_1\sigma_2\rho \\ -\sigma_2\sigma_1\rho & \sigma_2^2 \end{bmatrix} \begin{bmatrix} \frac{1}{2} & \frac{1}{2} \\ -1 & 1 \end{bmatrix}^T \qquad \text{(D-9)}$$

$$= \exp\left[-\frac{(t-\tau)}{t_c}\right] \begin{bmatrix} \frac{1}{4}\left(\sigma_1^2 + \sigma_2^2 - 2\rho\sigma_1\sigma_2\right) & \frac{1}{2}\left(\sigma_2^2 - \sigma_1^2\right) \\ \frac{1}{2}\left(\sigma_2^2 - \sigma_1^2\right) & \sigma_1^2 + \sigma_2^2 + 2\rho\sigma_1\sigma_2 \end{bmatrix} .$$

Now since $\sigma_1 = \sigma_2$ from Eq. (D-4), $\delta\theta_1$ and $\delta\theta_2$ must be <u>independent</u>.

Further, if the value of $\rho = 0.5$ is substituted, Eq. (D-9) reduces to

$$\mathcal{E}\left[\delta\theta(t)\delta\theta^T(t+\tau)\right] = \exp\left[-\frac{(t-\tau)}{t_c}\right]\begin{bmatrix}\frac{1}{4}\sigma_1^2 & 0\\ 0 & 3\sigma_1^2\end{bmatrix} \qquad \text{(D-10)}$$

The horizon errors for θ_1 and θ_2 can thus be simulated by two independent processes whose variances are $\sigma_1^2/4$ and $3\sigma_1^2$, respectively, and whose equivalent time constant is t_c. By an identical analysis, the horizon errors for θ_1' can be simulated by a process with the same statistics as the process for θ_1. Although there may be correlation between θ_1 and θ_1', they were assumed to be independent. This assumption was made because sufficient data were not available to realistically simulate these correlations.

In summary then, the contribution of the horizon errors can be modeled by three independent Markov processes. From Eq. (D-10) formulas for generating the instantaneous values of these errors can readily be found. Specifically, if $x_1, x_2, \ldots, x_6$ are reserved for the inertial position and velocity states of the navigator, and x_7, x_8, x_9 are used to denote the states for these biases, it can be shown that

$$\begin{aligned}
\dot{x}_7 &= -x_7/625 + u_7, \quad \mathcal{E}\left[x_7^2(0)\right] = \sigma_1^2/4 = .01485^2\\
\dot{x}_8 &= -x_8/625 + u_8, \quad \mathcal{E}\left[x_8^2(0)\right] = \sigma_1^2/4 = .01485^2 \qquad \text{(D-11)}\\
\dot{x}_9 &= -x_9/625 + u_9, \quad \mathcal{E}\left[x_9^2(0)\right] = 3\sigma_1^2 = .05145^2
\end{aligned}$$

where u_7, u_8, u_9 are zero mean white noise processes whose variances are

$$\mathcal{E}[u_7(t)u_7(\tau)] = \frac{2}{625}(.01485)^2\delta(t-\tau)$$

$$\mathcal{E}[u_8(t)u_8(\tau)] = \frac{2}{625}(.01485)^2\delta(t-\tau) \qquad \text{(D-12)}$$

$$\mathcal{E}[u_9(t)u_9(\tau)] = \frac{2}{625}(.05145)^2\delta(t-\tau)$$

and $\delta(t-\tau)$ is the Dirac delta function.

APPENDIX E

ONE-WAY DOPPLER MODELING

As indicated in Sect. 8.1, the Kalman filter formulation cannot directly accommodate measurements which are functions of the states at different times. The three methods of obtaining compatibility which were used in this study are described in detail here.

E.1 ACQUISITION RANGE REFERENCE METHOD (P. Soule, Ref. 41)

In the acquisition range reference method the time t_i in Eq. (8-4) is fixed at t_0, the time of acquisition of a ground station, and the corresponding range, $\rho(t_0)$, is made a state variable x_{15}. Then with measurements being taken at $t_1, t_2, \ldots, t_k$ as the satellite passes over the ground station, the data

$$\begin{aligned} y_1 &= \rho(t_1) + x_7(t_1) - x_{15} - x_7(t_0) + v_1 \\ y_2 &= \rho(t_2) + x_7(t_2) - x_{15} - x_7(t_0) + v_2 \\ &\cdots \\ y_k &= \rho(t_k) + x_7(t_k) - x_{15} - x_7(t_0) + v_k \end{aligned} \qquad \text{(E-1)}$$

readily conform to the usual Kalman filter formulation. It is noted that, since the state $\rho(t_0)$ is perfectly correlated with the position states of the satellite and the ground station at t_0, the correct state covariance matrix at t_0 will be positive semidefinite. In theory, however, there should be no difficulty processing the data since, as Kalman and Bucy (Ref. 29) point

out, the Riccati equation will converge to a unique solution even with a positive semidefinite initial condition under very general conditions.

The correct covariance matrix at acquisition is constructed from the propagated state covariance matrix by first zeroing out all rows and columns beyond six. The variances for states x_7, x_8, . . . , x_{14}, x_{16} are then reset to their initial values, forming a temporary covariance matrix, $\bar{P}_k$. Now, as indicated above, the desired covariance matrix must contain terms to account for the correlation that exists between the navigator's position and the range at acquisition, x_{15}. This matrix, P_k^+, can be computed directly from the relationship

$$P_k^+ = F\, P_k^-\, F^T$$

where the transformation matrix F is defined by

$$\hat{x}_k^+ = F\, \hat{x}_k^- \qquad \text{(E-2)}$$

with

$\hat{x}_k^+$ = the state vector immediately after acquisition

$\hat{x}_k^-$ = the state vector immediately before acquisition

$$F = \frac{\partial \hat{x}_k^+}{\partial \hat{x}_k^-} = \left[\begin{array}{ccc|c} & I_{14\times 14} & & 0_{14\times 2} \\ \hline \frac{\partial \hat{x}_{15}}{\partial \hat{x}_1} & \frac{\partial \hat{x}_{15}}{\partial \hat{x}_2} & \cdots & \frac{\partial \hat{x}_{15}}{\partial \hat{x}_{16}} \\ \hline & 0_{1\times 14} & & 0 \quad 1 \end{array}\right] \qquad \text{(E-3)}$$

and

$$\hat{x}_{15} = \rho(t_0) = \left[\left(\hat{x}_1 - \hat{x}_9\right)^2 + \left(\hat{x}_2 - \hat{x}_{10}\right)^2 + \left(\hat{x}_3 - \hat{x}_{11}\right)^2\right]^{1/2}$$

i.e., F is the 16 × 16 identity matrix with the 15th row reset as indicated.

It should be noted that this type of re-initialization technique can be useful for other sensors as well. In particular, it can be used when a new state variable, which is introduced at an arbitrary sample time, has a functional dependence on other estimated state variables that are continuously included in the dynamical model. Specifically, this same technique has proved very useful in the initialization of the covariance matrix for unknown landmarks, especially when the state vector included several biases from multiple sensor types. When compared to the conventional methods of calculating the covariance terms in previous studies (Refs. 4, 5, and 17), the technique suggested here appears to be much more systematic, thereby preventing inadvertent omissions of necessary terms.

E.2 PREVIOUS RANGE REFERENCE METHOD (I. A. Gura)

In the previous range reference method, the necessity for the state x_{15} and the accompanying covariance initialization process can be eliminated by choosing t_i in Eq. (8-3) to be the time of the previous measurement. Thus,

$$\begin{aligned}
y_1 &= \rho(t_1) - \rho(t_0) + x_7(t_1) - x_7(t_0) + v_1 - v_0 \\
y_2 &= \rho(t_2) - \rho(t_1) + x_7(t_2) - x_7(t_1) + v_2 - v_1 \\
&\;\;\vdots \qquad\qquad \vdots \qquad\qquad \vdots \\
y_k &= \rho(t_k) - \rho(t_{k-1}) + x_7(t_k) - x_7(t_{k-1}) + v_k - v_{k-1}
\end{aligned} \tag{E-5}$$

In order to show that this formulation can be accommodated by the Kalman filter algorithm, note that the predicted measurement can be expressed as:

$$\hat{y}_k = \rho(\hat{x}_{k/k-1}) - \rho(\hat{x}_{k-1/k-1}) \tag{E-6}$$

where $\hat{x}_{k-1/k-1}$ is the estimated state at t_{k-1} based on data taken to t_{k-1}, and $\hat{x}_{k/k-1}$ is the estimated state at t_k based on data taken to t_{k-1}. That is,

$$\hat{x}_{k/k-1} = g(\hat{x}_{k-1/k-1}) \tag{E-7}$$

where g ( ) is the vector function symbolizing a one step integration of the state vector.

Now,

$$\hat{x}_{k-1/k-1} = g^{-1}(\hat{x}_{k/k-1}) \tag{E-8}$$

where the notation g^{-1} ( ) is used to indicate a one step backwards integration.

Thus Eq. (E-6) becomes

$$y_k = \rho\left(\hat{x}_{k/k-1}\right) - \rho\left[g^{-1}(\hat{x}_{k/k-1})\right] \tag{E-9}$$

which is clearly within the domain of the filter algorithm. From Eq. (E-9) the measurement partials can readily be derived to be

$$\frac{\partial \hat{y}_k}{\partial x} = \frac{\partial \rho(\hat{x}_{k/k-1})}{\partial x} - \frac{\partial \rho}{\partial g^{-1}} \frac{\partial g^{-1}}{\partial x} = \frac{\partial \rho(\hat{x}_{k/k-1})}{\partial x} - \frac{\partial \rho}{\partial g^{-1}} \Phi^{-1}(k+1,k) \tag{E-10}$$

where $\Phi(k+1,k)$ is the transition matrix for the state vector in question.

Note from Eq. (E-5) that the measurement noise is not white as is required for the Kalman filter. That is, if

$$\mathcal{E}\left(v_k^2\right) = R$$

$$\mathcal{E}\left(v_k - v_{k-1}\right)^2 = 2R \qquad \text{(E-11)}$$

$$\mathcal{E}(v_k - v_{k-1})\,(v_j - v_{j-1}) = \begin{cases} 2R & j=k \\ -R & j=k-1 \text{ or } k+1 \\ 0 & \text{for all other } j \end{cases}$$

For the problem at hand however, R is quite small relative to other variances, and this effect should be insignificant if ignored. This contention was tested in with the simulation program and found to be quite valid (See Section 8.7).

E.3 RANGE RATE AT MIDPOINT

Consider Eq. (E-5). A simple approach to data processing would be to model the data using the range rate at the midpoint of the interval in question.

That is, the data actually processed becomes

$$\bar{y}_k = y_k - y_{k-1} \qquad \text{(E-12)}$$

while the predicted measurement in the filter is the instantaneous range rate at $(t_k + t_{k-1})/2$, multiplied by the interval length $t_k - t_{k-1}$. The measurement equation thus becomes

$$\bar{y}_k = \{\dot{\rho}[(t_k + t_{k-1})/2] + x_8\}\,(t_k - t_{k-1}) + v_k - v_{k-1} \qquad \text{(E-13)}$$

Although such modeling may be intuitively appealing, the degradation in performance was shown to be considerable when $t_k - t_{k-1}$ was more than five seconds (see Section 8.8).

APPENDIX F

LOCATIONS FOR KNOWN LANDMARKS (GROUND STATIONS)

STATION	GEOCENTRIC LATITUDE	EAST LONGITUDE
1	-23.2	314.1
2	40.7	141.3
3	61.2	210.1
4	76.5	291.2
5	-77.8	166.6
6	-4.6	55.4
7	32.2	253.2
8	51.1	358.9
9	39.1	283.1
10	-34.6	138.6
11	-25.9	28.3
12	-14.3	189.2
13	14.9	120.0
14	30.3	262.2
15	34.5	69.2
16	34.1	240.8
17	19.2	166.6
18	18.7	98.9
19	63.9	337.4
20	47.3	306.0
21	35.1	33.3
22	66.5	210.0
23	69.5	260.0
24	60.0	195.0
25	60.0	240.0

STATION	GEOCENTRIC LATITUDE	EAST LONGITUDE
26	60.0	285.0
27	60.0	0.0
28	45.0	150.0
29	45.0	255.0
30	45.0	285.0
31	30.0	135.0
32	30.0	36.0
33	15.0	150.0
34	15.0	210.0
35	15.0	330.0
36	15.0	15.0
37	15.0	45.0
38	15.0	90.0
39	0.0	135.0
40	0.0	165.0
41	0.0	195.0
42	0.0	285.0
43	0.0	315.0
44	0.0	15.0
45	0.0	45.0
46	0.0	105.0
47	-15.0	135.0
48	-15.0	300.0
49	-15.0	15.0
50	-15.0	45.0
51	-30.0	135.0
52	-30.0	180.0
53	-30.0	300.0
54	-30.0	15.0
55	-45.0	172.0

STATION	GEOCENTRIC LATITUDE	EAST LONGITUDE
56	-66.5	105.0
57	-66.5	60.0
58	-66.5	90.0
59	66.5	225.0
60	66.5	15.0
61	60.0	225.0
62	60.0	255.0
63	60.0	315.0
64	60.0	15.0
65	45.0	240.0
66	45.0	270.0
67	45.0	0.0
68	30.0	180.0
69	30.0	75.0
70	15.0	180.0
71	15.0	300.0
72	15.0	0.0
73	15.0	30.0
74	15.0	75.0
75	0.0	120.0
76	0.0	150.0
77	0.0	180.0
78	0.0	285.0
79	0.0	300.0
80	0.0	0.0
81	0.0	30.0
82	0.0	75.0
83	-15.0	120.0
84	-15.0	285.0
85	-15.0	315.0

STATION	GEOCENTRIC LATITUDE	EAST LONGITUDE
86	-15.0	30.0
87	-30.0	120.0
88	-30.0	150.0
89	-30.0	285.0
90	-30.0	315.0
91	-30.0	30.0
92	-45.0	285.0
93	-66.5	120.0
94	-66.5	300.0
95	10.0	250.0
96	-15.0	210.0
97	-23.5	225.0
98	-23.5	240.0
99	-23.5	255.0
100	-37.0	210.0
101	-47.0	27.5
102	-47.0	52.5
103	-47.0	67.5
104	-53.0	330.0

REFERENCES

1. A. S. Abbott, The Aerospace Corporation, El Segundo, California.

2. Angus Andrews, "A Square Root Formulation of the Kalman Covariance Equations," AIAA Journal, 1165-66, June 1968.

3. R. H. Battin, Astronautical Guidance, McGraw-Hill Book Company, New York, New York, 1964.

4. J. F. Bellantoni, "Unidentified Landmark Navigation," AIAA Journal, 5 (8), 1478, 1967.

5. W. L. Brogan, "Unknown Landmark Tracking for Orbit Navigation," two-week short course: Space Navigation and Guidance, University of California Extensions, Los Angeles, California, October 16-27, 1967.

6. W. L. Brogan, A Study of Autonomous Navigation Utilizing Known Landmark Tracking, Report No. TOR-1001(2555)-3, The Aerospace Corporation, El Segundo, California, December 1966.

7. W. L. Brogan and J. L. LeMay, "Autonomous Orbit Determination at Synchronous Altitude," AAS Paper No. 68-129, AAS/AIAA Astrodynamics Specialist Conference, Jackson, Wyoming, September 3-5, 1968.

8. R. Grover Brown, Analysis of an Integrated Inertial/Doppler-Satellite Navigation System, Report No. ERI-62600, Engineering Research Institute, Iowa State University, Ames, Iowa, December 1969.

9. G. Buechler and Dennis C. Walker, TRACE-66 Orbit Determination Program, Volume III: Trajectory Generation Equations and Methods, Report No. TOR-0066(9320)-2, Vol. III, The Aerospace Corporation, El Segundo, California, April 1970.

10. R. W. Davis, et al., Lockheed Missiles and Space Company, Sunnyvale, California.

11. J. C. Devolites, et al., IBM Corporation, Owego, New York.

12. H. L. Dibble, Air Force Avionics Laboratory, Wright-Patterson Air Force Base, Ohio.

13. R. J. Farrar, Advanced Missions Operations Concepts, USAF/NASA Task 4, Vol. IV: Special Study, Survey of Autonomous Navigation Methods for NASA STS Advanced Mission, Report No. TOR-0059(6759-05)-1, Vol. IV, The Aerospace Corporation, El Segundo, California, July 1970.

14. J. J. Fischer and K. C. Kochi, Onboard Orbital Navigation Using Unknown Landmarks, Report No. TR-1855/311, Autonetics Division North American Rockwell, Downey, California.

15. R. J. Fitzgerals, Studies in Orbit Navitation and Optimal Filtering, Report No. U67-4086-1, Raytheon Company, Sudburg, Massachusetts, October 1967.

16. D. J. Griep, "Low Frequency Horizon Sensor Noise Model," ATM-69(4306-02)-1, The Aerospace Corporation, El Segundo, California, November 1968 (internal correspondence; not available outside The Aerospace Corporation).

17. W. H. Guier and R. R. Newton, The Earth's Gravity Field Deduced from the Doppler Tracking of Five Satellites, Report No. TD-634, The Johns Hopkins University Applied Physics Laboratory, Silver Springs, Maryland, December 1964.

18. I. A. Gura, "Extension of Linear Estimation Techniques to Nonlinear Problems," The Journal of the Astronautical Sciences, XV, (4), 194-206, July-August 1968.

19. I. A. Gura and A. B. Bierman, On Computational Efficiency of Linear Filtering Algorithms, Report No. TR-0059(6521-01)-1, The Aerospace Corporation, El Segundo, California, November 1970; also to be published in Automatica.

20. T. L. Gunckel II, "Orbit Determination Using Kalman's Method," Journal of Institute of Navigation, 10, (3), Autumn 1963.

21. H. T. Hendrickson, A Study of an Autonomous Unknown Landmark Tracking Navigation System, Report No. TR-0059(6311)-4, The Aerospace Corporation, El Segundo, California, February 1971; also presented at Institute of Navigation Meeting, Huntsville, Alabama, February 23-25, 1971.

22. H. T. Hendrickson, A Study of an Unknown Landmark Tracking Navigation System--First Set of Results, Report No. TOR-0059(6311)-18, The Aerospace Corporation, El Segundo, California, December 1970.

23. H. T. Hendrickson, A Study of an Unknown Tracking Navigation System--Second Set of Results, Report No. TOR-0059(6311)-20, The Aerospace Corporation, El Segundo, California, January 1971.

24. H. T. Hendrickson, A Study of a Horizon Scanner Autonomous Orbital Navigation System, Report No. TOR-0059(6311)-11, The Aerospace Corporation, El Segundo, California, August 1970.

25. H. T. Hendrickson, Orbit Navigation Analysis Program (ONAP) Structure and Flow, Report No. TOR-0059(6311)-9, The Aerospace Corporation, El Segundo, California, August 1970.

26. H. T. Hendrickson, The Simplified Orbit Navigation Analysis Program, Report No. TOR-0059(6311)-10, The Aerospace Corporation, El Segundo, California, August 1970.

27. J. R. Janus and J. L. LeMay, Error Analyses of Self-Contained Orbit Navigation Systems, Report No. TOR-469(5540-10)-6, The Aerospace Corporation, El Segundo, California, December 1964.

28. Keith Joseph, Space Shuttle Horizon Sensor Navigation Analysis, Report No. 14492-6001-R0-00, TRW Systems Group, Redondo Beach, California, October 1970.

29. R. E. Kalman and R. S. Bucy, "New Results in Linear Filtering and Prediction Theory," Transactions of ASME (Journal of Basic Engineering), 83D, 95-108, March 1961.

30. D. G. King-Hele, G. E. Cook, and Margaret H. Watson, "Even Zonal Harmonics in the Earth's Gravitational Potential," Nature, 202, 996, June 6, 1964.

31. A. L. Knoll and M. M. Edelstein, "Estimation of Local Vertical and Orbital Parameters for an Earth Satellite Using Horizon Sensor Measurements," AIAA Journal, 3, (2), 338-45, February 1965.

32. G. M. Levine, "A Method of Orbital Navigation Using Optical Sightings to Unknown Landmarks," AIAA/ION Guidance and Control Conference, August 1965.

33. J. L. LeMay, J. S. Meditch, and A. R. Stubberud, "Design and Application of a Digital Computer Program for Error Analysis of a Wide Class of Orbit Navigation Systems," Third Congress of the International Federation of Automatic Control, London, England, June 20-25, 1966.

34. W. G. McArthur, "Horizon Sensor Navigation Errors Resulting from Statistical Variations in the CO_2 14-16 Micron Radiation Band," Ninth Symposium on Ballistic Missile and Space Technology, San Diego, California, August 1964.

35. J. S. Meditch, J. L. LeMay, and J. P. Janus, Analysis of a Horizon Scanner Autonomous Orbital Navigation System, Report No. TOR-469(5540-10)-6, The Aerospace Corporation, El Segundo, California, July 1965.

36. J. S. Meditch and W. L. Brogan, Description of the Orbit Navigation Program (ONAP), Report No. TOR-1001(2555)-2, The Aerospace Corporation, El Segundo, California, April 1966.

37. B. J. Miller and A. S. Abbott, Observation Theory and Sensors, Report No. SID 65-1200-2, North American Aviation, Inc., Downey, California, December 1965.

38. E. S. Muller and P. M. Kachmar, "A New Approach to On-Board Orbit Navigation," presented at Institute of Navigation Meeting, Huntsville, Alabama, February 23-25, 1971.

39. J. H. Neally, M. J. Rademacher, and W. F. Rearick, The Modularized Vehicle Simulation (MVS) System, Report No. TOR-0158(3307-02)-2, The Aerospace Corporation, El Segundo, California, February 1968.

40. L. Schusterman, "Variable Scale Height Atmospheric Density Models," ATM-71(6472)-53, The Aerospace Corporation, El Segundo, California, January 1971 (internal correspondence; not available outside The Aerospace Corporation).

41. Peter Soule, "Use of Transit Signals for Satellite Navigation," private correspondence from McDonnell-Douglas, Houston, Texas, December 1970.

42. C. C. Tonies, TRACE Orbit Determination Program, Version D, Report No. TR-669(9990)-3, The Aerospace Corporation, El Segundo, California, September 1966.

43. U. S. Committee on Extension to the Standard Atmosphere, U.S. Standard Atmosphere, 1962, Government Printing Office, Washington, D.C., 1962.

44. J. B. Woodford, W. C. Melton, and R. L. Cutcher, "Satellite Systems for Navigation Using 24-Hour Orbits," Eastcon '69 Convention Record, IEEE Transactions on Aerospace and Electronic Systems, Washington, D.C., October 27-29, 1969; also Report No. SAMSO TR-69-423, January 30, 1970.

45. General Electronic Company, Syracuse, New York.

46. Quantic Industries Mod. IV High-Accuracy, High-Reliability Horizon Sensor System, Report No. ETD-321A, Quantic Industries, Inc., San Carlos, California, April 1970.

47. Standardized Space Guidance Study (SSGS): Program Definition Study, IA, Report No. SSD-TDR-64-131, Sperry Gyroscope Company, Great Neck, New York, May 1964.

48. Standardized Space Guidance Study (SSGS): Phase IA Study, Report No. SSD-TDR-64-129, Autonetics Division North American Aviation, Inc., Downey, California, May 1964.

49. Standardized Space Guidance Study (SSGS): Program Definition Studies, Report No. 3-260-8283, IBM Federal Systems Division, IBM Corporation, Owego, New York, May 1964.

50. Standardized Space Guidance Study (SSGS): Final Report for Phase IA Standardized Space Guidance Study, Report No. SSD-TDR-64-132, TRW Systems Group, Redondo Beach, California, May 1964.

51. Standardized Space Guidance Study (SSGS): Advanced Development Program Definition Study, MIT Instrumentation Laboratories, Boston, Massachusetts, June 1964.

52. Tisnart Engineering Analysis Report, Report No. LMSC-A854608, Contract No. AF04(695)-860 CCN-25, Lockheed Missiles and Space Company, Sunnyvale, California, March 30, 1967.